Rochester Institute of Technology

RIT Digital Institutional Repository

2002

Analysis of the droplet size reduction in a pMDI to the addition of a turbulence generating nozzle

Michael Medlar

ANALYSIS OF THE DROPLET SIZE REDUCTION IN A pMDI DUE TO THE ADDITION OF A TURBULENCE GENERATING NOZZLE

by

Michael P. Medlar

A Thesis Submitted in
Partial Fulfillment of the
Requirement for the

MASTER OF SCIENCE
IN
MECHANICAL ENGINEERING

Approved by:

Dr. Risa Robinson
Department of Mechanical Engineering

_____
(Thesis advisor)

Mr. John Wellin
Department of Mechanical Engineering

_____

Dr. Jeffrey Kozak
Department of Mechanical Engineering

_____

Dr. Edward C. Hensel
Department Head of Mechanical Engineering

_____

DEPARTMENT OF MECHANICAL ENGINEERING
ROCHESTER INSTITUTE OF TECHNOLOGY
November, 2002

THESIS REPRODUCTION PERMISSION STATEMENT

Permission granted

ANALYSIS OF THE DROPLET SIZE REDUCTION IN A pMDI DUE TO THE ADDITION OF A TURBULENCE GENERATING NOZZLE

Abstract

Pharmaceutical inhalation aerosol technology has become an important therapy for the treatment of both respiratory and non-respiratory illness. Targeting therapeutic aerosols to the small airways of the lung can effectively treat many of these diseases. Delivery of the therapeutic agent directly to the site of action, for cases involving respiratory diseases, ensures an adequate therapeutic level of the drug is reached, without leading to side effects due to high systemic concentrations. For non-respiratory diseases, the periphery of the lung offers enormous surface area (approximately $100m^2$) for rapid absorption into circulation. In either case, the appropriate spray characteristics ($0.5~\mu m < MMAD < 5~\mu m$ and a low velocity) are vital to targeting the lung periphery.

In inhalation technology, specifically pressurized metered dose inhalers (pMDI), many factors lead to the break-up or atomization of the formulation. These could include the nozzle geometry, volatilization of the propellant (cavitation), and turbulence in the nozzle. The purpose of this study was to design and analyze turbulence generating nozzles for the improvement of existing pressurized metered dose inhaler therapy. The existence of turbulence within the inhaler nozzle is one mechanism that leads to the production of the aerosol in this device. The current inhaler internal flow passage was analyzed on a turbulence basis and a baseline median representative droplet size was predicted using the Huh atomization model. The analysis of this atomization model led to the conclusion that changing the turbulence exit conditions in the inhaler through the addition of a nozzle could lead to a reduced median secondary droplet size. To investigate this, simple nozzles were designed to produce a turbulent flow condition on exit from the orifice. The flow condition was analyzed using computational fluid dynamics software (CFD). The average turbulent kinetic energy (k_{avg}) and turbulent kinetic energy dissipation rate (ε_{avg}) on exit from the orifice were related to a representative secondary droplet size distribution using the Huh atomization model. The nozzle with the largest potential (i.e. lowest median secondary drop size) was optimized in 3D and a resulting median secondary drop size was predicted. Development of the proper turbulence characteristics with this add-on nozzle led to a 15.5% improvement of the representative secondary median droplet size based on turbulence effects alone.

Table of Contents

Figures and Tables

Figures

Tables

Variables and Abbreviations

Variables

C	Normalization constant
C_k, C_μ, C_ε, $C_{\varepsilon 1}$, $C_{\varepsilon 2}$	Constants in the k-e turbulence model
D	Any relevant diameter
F(x)	Cumulative distribution function
g	Gravitational acceleration
h	Any relevant parameter or dimension
I	Turbulent intensity
k	Turbulent kinetic energy
L	Any relevant length scale
Oh	Ohnesorge number
P	Pressure
$\overline{P}$	Mean Pressure
p(x)	Probability density function
Re	Reynolds number
s	Any relevant parameter or dimension
t	Time
U	Any mean velocity
u	Instantaneous velocity component
$\overline{u}$	Mean velocity component
u'	Fluctuating velocity component
x	Independent variable, secondary drop diameter
$\phi(x)$	Turbulence energy spectrum
ε	Turbulent kinetic energy dissipation rate
λ	Wave number
μ	Dynamic viscosity
ρ	Density
τ	Shear stress, any relevant time scale
$\overline{\tau}$	Mean shear stress
$\overline{\tau}^t$	Reynolds stress

Abbreviations and Subscripts

Avg	Average
CF	Cystic Fibrosis
CFD	Computational Fluid Dynamics
DPI	Dry Powder Inhaler
MMAD	Mass Median Aerodynamic Diameter
Multi	Multiple
PDF	Probability Density Function
pMDI	Pressurized Metered-Dose Inhaler

Ver	Version
A	Atomization
e	Eddy
f	Fluid
g	Gas
o	Initial
t	Turbulence
w	Wave growth

Chapter 1-Introduction

1.1 Overview

In the treatment of both respiratory and non-respiratory diseases, aerosol administration represents a valuable means by which a therapeutic agent may be delivered. To manage these illnesses effectively, the drugs must be targeted to the appropriate therapeutic or biological site of action. In many cases, the suitable site of action is the small airways of the lung. To target the lung periphery, the therapeutic aerosol must have the appropriate spray characteristics (mass median aerodynamic diameter between 0.5 µm and 5 µm[1,2,3,4] and as low a velocity as possible). The objective of this study is to design and analyze an atomizing nozzle for the purposes of improving Pharmaceutical Aerosol Inhalation Technology. Existing means of inhalation devices include Pressurized Metered-Dose Inhalers (pMDI), Dry Powder Inhalers (DPI), and Nebulizers. In this investigation, an add-on atomizing nozzle was designed based on the concepts behind turbulence generation and the Huh Atomization Model[5] to improve existing pMDI therapy. A computational fluid dynamic analysis was done using a commercial software package to ensure that the atomizing nozzle design enhanced the spray characteristics from the pMDI (namely, reduced the median droplet size at a similar exit velocity).

1.2 Review of Medical Inhalation Therapy

Pharmaceutical Inhalation Aerosol Technology has become an important therapy for the treatment of both respiratory and non-respiratory illness. Targeting therapeutic aerosols to the small airways of the lung can effectively treat many of these diseases. Delivery of the therapeutic agent directly to its site of action, which is the case in respiratory diseases, ensures that an adequate therapeutic level of the drug is reached, without leading to side effects due to high systemic concentrations. For non-respiratory diseases, the periphery of the lung offers enormous surface area (approximately $100m^2$) for rapid absorption into circulation.[6] In either case, this route of delivery represents a valuable means by which diseases may be treated.

1.2.1 Respiratory Disease Treatment

In respiratory diseases, the small airways are prone to a variety of diseases. Small airway disease is a significant component of obstructive airway pathology. Emphysema, asthma, bronchiectasis, extrinsic allergic alveolitis, sarcoidosis, cancer, and bacterial infections due to Cystic Fibrosis can all involve the small airways.[7,8,9] To treat these diseases, drugs must be effectively delivered to the small airways.

The treatment of asthma is a valid example. As indicated by Howarth[10], asthma is a chronic inflammatory disease characterized by airway obstructions of varying degrees and bronchial hyper-responsiveness. Thus, it can be treated with corticosteroids that have anti-inflammatory activity and bronchodilators. Inhaled bronchodilator therapies are targeted at certain drug receptors called B_2-adrenoceptors. These receptors are not evenly distributed throughout the respiratory tract. The highest density of B_2 receptors are found in the alveolar walls in the lung periphery.[11] In order to treat asthma effectively with bronchodilators, the drug must be delivered to the lower airways.

Cystic Fibrosis, CF, is another good example. According to Toso, Williams, and Noone[8] CF is a heterogeneous, autosomal recessive genetic disorder characterized by abnormalities in exocrine gland function. The disease affects multiple organ systems, including gastrointestinal, pulmonary, and reproductive systems. Progressive pulmonary disease is a major cause of death. Bacterial infections play a central role in the progression of lung disease in CF. They lead to progressive lung destruction, deterioration in lung function, and eventual respiratory failure. Given this fact, antibiotics are a primary component of therapy. Systemic antibiotic therapy usually leads to clinical improvement, but the effect on bacterial colonization is variable and often transient. Direct delivery of antibiotics to the lower airways by aerosol administration has a number of theoretical advantages over the systemic route. First, inhalation allows for deposition of antibiotics at the site of infection where high drug concentrations are needed to inhibit bacterial growth. And second, aerosols permit lower drug doses without a compromise in efficacy, and this may reduce systemic side effects and ultimately be more cost effective.

The lungs are a common site for primary malignancies or cancer. Sharma et al[7] suggests that one potential treatment approach is targeted dose intensification using inhaled chemotherapy for regional therapy. This type of therapy could achieve high levels of the

drugs in pulmonary tissues without subjecting the patients to major surgical procedures and keeping systemic side effects low. The total amount of drug required to adequately expose the entire lung by inhalation is a small fraction of that required by the oral route. Drugs delivered to the lung will most likely reach their tumors through the local blood supply.[7] Pulmonary vasculature forms a separate circuit from the systemic circulation. The main pulmonary artery starts in the right ventricle and then divides into two branches for the right and left lungs. The branching continues until a fine capillary bed is formed at the level of the alveolar walls.[12] So, to treat lung cancer effectively, in this context, drugs must be delivered to the alveoli or the lung periphery.

1.2.2 Non-respiratory Disease Treatment

For non-respiratory disease treatment, pulmonary drug delivery offers two distinct advantages for certain scenarios. First, pulmonary delivery offers a non-invasive option for systemic therapy with large molecules such as insulin, growth hormone, interferons, calcitonin, and erythropoietin.[6] Often times, these drugs are injected and can't be taken orally because enzymes in the stomach destroy the drugs. The inhalation route provides an alternative to injections. Second, inhalation delivery can provide more rapid absorption into systemic circulation than can be achieved by other non-invasive routes of delivery. The lungs are efficiently permeable for delivering these macromolecules into circulation.[6] The alveolar region is the target area for the deposition of drugs intended to have a rapid systemic effect because absorption from this region is so efficient.[13] This region has an effective surface area of around $100m^2$.[6] Large drug particles are transported fairly rapidly across the impermeable cell membrane of this region by a bucket brigade of tiny membrane bubbles, or transcytotic vesicles, formed by invagination of the cell membrane.[6] The alveolar space in the lung is used as a portal to systemic circulation and drugs must be delivered effectively to this region to treat non-respiratory diseases appropriately.

1.3 Review of Current Inhalation Devices

There are three major categories of medical inhalation devices currently in use. All of them have their advantages and drawbacks. They consist of the Pressurized Metered-Dose Inhaler (pMDI), the Dry Powder Inhaler (DPI), and the Nebulizer.

1.3.1 Pressurized Metered-Dose Inhaler (pMDI)

The fundamental components of the pMDI are illustrated in Figure 1.1. They include an actuator, metering chamber, and a pressurized container or canister that contains the drug suspension or solution, propellant, and surfactant. This device is relatively small, easy to handle, portable, and inexpensive however, it has certain limitations. Often there is poor coordination between actuation and inhalation in some patients leading to poor drug delivery. Also, these devices initially release large droplets at high velocities. The droplets/particles start with a MMAD around 35 μm and a velocity of 15-30 m/s on exit from the inhaler.[1,14,15,16,17] It isn't until a distance of around 10-12 cm downstream from the nozzle that they reach a mass median aerodynamic diameter (MMAD) of 2-6 μm.[14,18] This leads to high oropharyngeal impaction of the droplets with only about ten percent of the dose ending up in the pulmonary airways.[1,14,18,19] There are certain accessory devices that have been developed to overcome many of these limitations. Spacers and valved holding chambers, when properly designed, reduce oropharyngeal deposition of the drug and reduce drug loss associated with poor hand-breath coordination.[14,20]
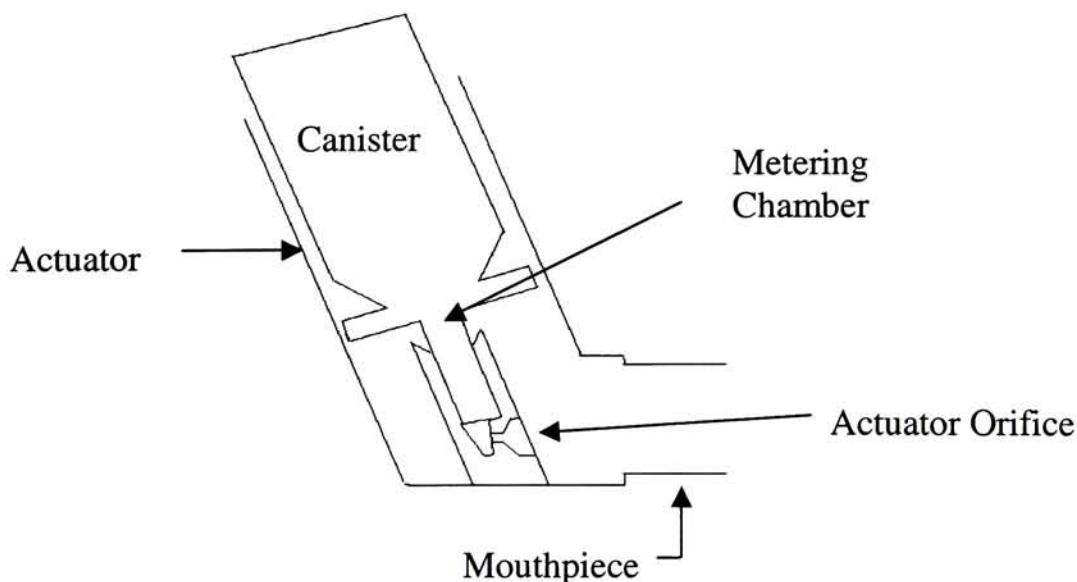
Figure 1.1. pMDI Schematic

1.3.2 Dry Powder Inhaler (DPI)

The drug in a dry powder inhaler is in the form of a finely milled powder in large aggregates, either alone or in combination with a carrier substance. These devices can be breath activated or take the form of a rotary planar configuration as in Figure 1.2. If breath activated, they rely on the patient's inspiratory flow to deaggregate and deliver the drug for inhalation. There is a need to generate a relatively high inspiratory flow (30-120 L/min) to release particles of a respirable size (MMAD < 5 μm) and achieve deposition in the alveolar space. [1,2,14,21,22,23,24] The high inspiratory flows required for optimal delivery have raised concerns about DPI effectiveness for patients with severe airway obstructions.[14] Due to their illness, these patients have difficulty developing the large flows. Also, dry powder inhalation is hindered by aggregation of small particles, which is exacerbated by the hygroscopic nature of the drug and its electrostatic charge. DPI's are only available with a few anti-asthma drugs and they are relatively expensive.[1]
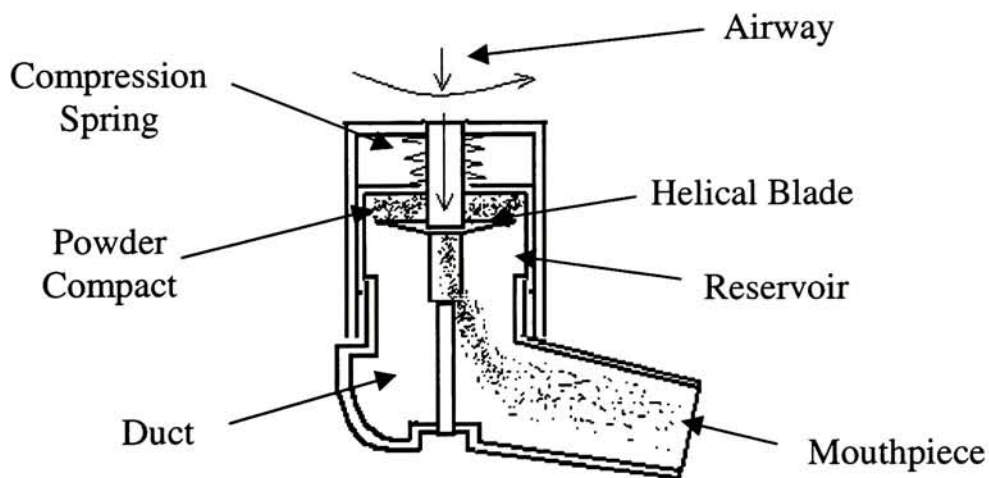
Figure 1.2. Rotary planer DPI[25]

1.3.3 Nebulizers

There are two types of nebulizers used to create an inhalation aerosol. They consist of the air-jet and ultrasonic types. Both nebulizer types require power sources to operate, they require a relatively large amount of time to deliver the drugs, and are also expensive.[17]

Jet Nebulizers work on a stream of compressed air or oxygen that is forced through a narrow tube that lies just above the surface of the liquid to be nebulized. The liquid is drawn

up by the Venturi effect and is fragmented into droplets by the high velocity jet of air as seen in Figure 1.3. They have baffles incorporated into their design so that most of the droplets delivered to the patient are within the respirable range of 1-5 μm (MMAD).[26] Only about ten percent of the drug is delivered to the lungs, eighty percent is trapped in the reservoir, tubing, and mask, and the rest is exhaled.
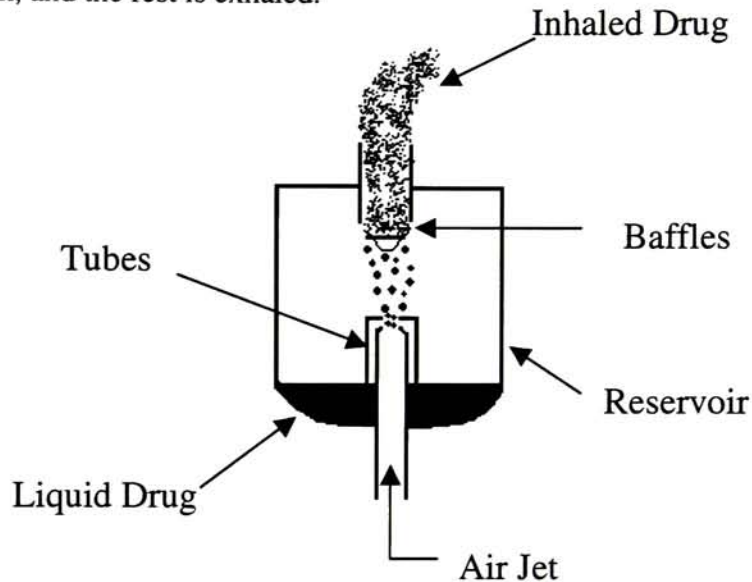
Figure 1.3. Jet Nebulizer [17]

Ultrasonic Nebulizers use vibrations by a piezoelectric crystal to produce the aerosol. They are quiet and there is little patient coordination required, however, they are prone to electrical and mechanical breakdown.[26] The ultrasonic nebulizer creates particle sizes of about 1–6 μm MMAD, depending on the manufacturer of the device.[26,27]
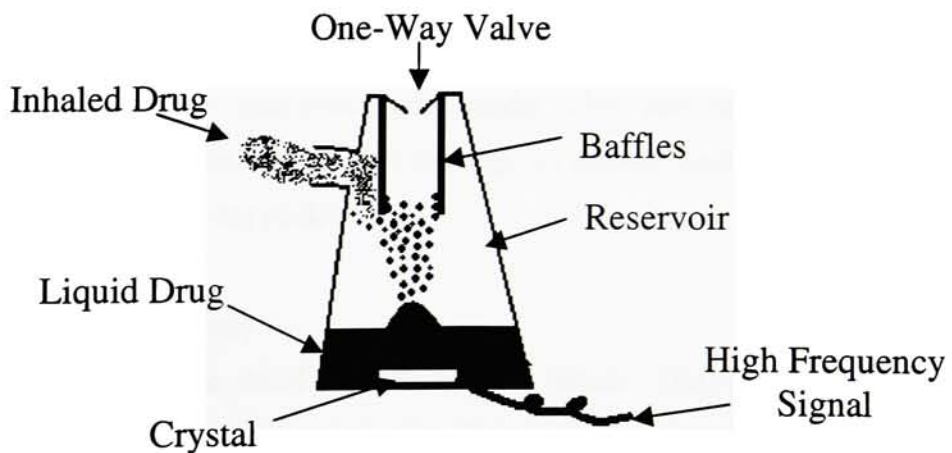
Figure 1.4. Ultrasonic Nebulizer [17]

Of the three inhalation devices described above, the pMDI is the most commonly prescribed method of aerosol delivery.[14,28] The pMDI is inexpensive, portable, and at least as effective as other systems of aerosol generation for drug delivery, if properly used.[14,29] Thus, with further improvements, it could become the most optimal and desirable means of drug delivery to the lungs.

1.4 Research Gaps

Pressurized Metered-Dose Inhalers have been around since the 1950's. Since their inception, numerous studies have been done to characterize their sprays using experimental techniques. These experimental techniques can be summarized as inertial impaction methods (impingers[30] and cascade impactors[31,32,33]), imaging methods (microscopy[34], high-speed photography[35], and holography[36]), and optical techniques (aerodynamic particle sizers[37,38,39] and laser light diffraction[40,41,42,43]). These experimental investigations are valuable, but they do not attempt to theoretically describe or model the pMDI spray. The literature suggests that analytical spray prediction models for the pMDI are not very abundant. Clark[44,45] has done work to study the atomization processes in the pMDI. More recently, Dunbar, Watkins, and Miller[46] have developed a theoretical model for the resulting spray from the pMDI. These investigations consider the flash evaporation of the propellant in the actuator nozzle as the primary atomization process.

This study is concerned with the positive results that turbulence generation can have on the spray resulting from the pMDI, thus, turbulence was considered as one of the factors contributing to the aerosol production in this device. The investigators mentioned previously did not consider turbulence in their pMDI spray model. They were not concerned with inducing additional turbulence into the flow (through an add-on nozzle) to improve the spray characteristics from the existing pMDI.

1.5 Scope of the Present Study

The aerosol production in the pMDI depends on many factors. They include volatilization (flashing) of propellant, formulation properties, flow passage geometry, and the turbulence characteristics at the nozzle exit. This study improves the pMDI by focusing on one of the

above processes in the nozzle design, namely, the turbulence characteristics at the nozzle exit. An add-on atomizing nozzle was designed to produce more favorable turbulence exit conditions than exist in current inhaler flow passages and reduce the resulting median droplet size. A computational fluid dynamic analysis was done to ensure that the atomizing nozzle design enhanced the turbulence exit characteristics. The Huh Atomization Model[5] was used to predict the spray distribution and illustrate a reduction in the median droplet size resulting from the add-on nozzle.

Chapter 2-Turbulence

2.1 Introduction

Turbulence can be defined as irregular fluid motion that results from the growth of disturbances and instability in laminar flow. Atomization is a disturbance growth process that converts a bulk liquid into a spray. So, it follows that development of the proper turbulence characteristics within our nozzle is a key factor in promoting greater atomization. In light of that fact, this chapter deals with turbulent internal flow, its characteristics, turbulence generation methods, and turbulent flow modeling.

2.2 What is Turbulence?

Turbulence is irregular fluid motion in which flow properties vary randomly in time at any given location in the flow field. Turbulent flow can be considered to consist of a fluctuating motion superimposed onto a mean one. Turbulence occurs via instabilities in laminar flow due to perturbations or disturbances. Turbulence arises at high Reynolds numbers due to greater tendency toward flow instability.[47] Perturbations and disturbances can only lead to turbulence if they are not damped out and allowed to grow. At higher Reynolds numbers viscosity's damping effects diminish so disturbances grow and break down into chaotic, sustained motion. Figure 2.1 shows the transition of the flow regime from laminar to turbulent with increasing Reynolds number. As Reynolds number is increased, fluctuations with the velocity in time grow as the flow enters a transitional state. Further increases in the Reynolds number lead to random velocity fluctuations and the onset of fully turbulent flow.
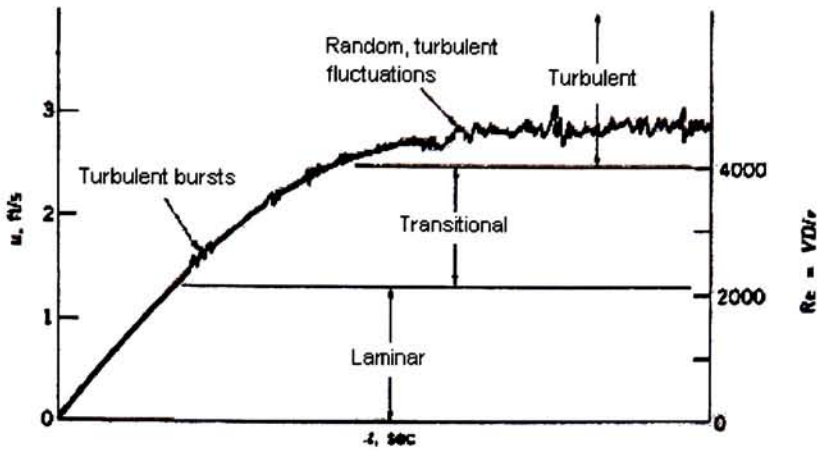
Figure 2.1. Transition from laminar to turbulent flow[48]

2.3 Characteristics of Turbulence

Every turbulent flow field is different. According to Richardson[48], the characteristics of each turbulent flow field depend on the conditions of the local environment in which the turbulence is generated. Most turbulent flows exhibit some general characteristics. First, turbulent flow is random and irregular. It is time and space dependent with a very large number of spacial degrees of freedom. A flow is not turbulent unless random velocity fluctuations are present at any given point. Second, turbulent flow is also three-dimensional and rotational. Turbulent flow contains intense, random vorticity fluctuations. Related to this concept of vorticity is the presence of eddies. An eddy is a large group of fluid particles that move laterally in the flow field while rotating, stretching, or breaking into more eddies. Turbulence involves the flow of eddies. Third, turbulent flow is inherently diffusive. The diffusivity of turbulence is what promotes mixing and increases momentum, heat, and mass transfer. Fourth, turbulent flow is dissipative. The kinetic energy of the turbulent flow dissipates into internal energy and eventually thermal energy due to the action of high viscous shear stresses on the fluid. Lastly, turbulent flow is a continuum. No section of the turbulent flow can be readily distinguished from its neighboring section.

The concepts of dissipation, diffusivity, and the flow of energy-containing eddies are important mechanisms in the atomization process detailed in the Huh atomization model[5] presented in Chapter 3.

2.4 Turbulence Generation Mechanisms

In internal fluid flow, there are three possible ways in which a turbulent flow condition can be created. First, rapid fluid flow past a wall can lead to unstable self-amplifying velocity fluctuations that form near the wall and spread to the remainder of the flow. Figure 2.2 illustrates how disturbances in the vicinity of the wall can upset the rest of the flow.
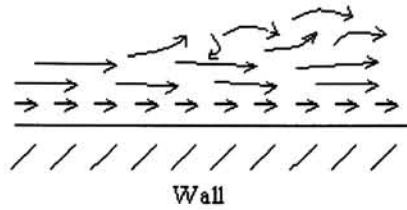
Figure 2.2. Rapid fluid flow past a wall

Second, velocity gradients between slow and fast moving fluid streams cause a shearing action leading to the production of turbulent eddies, as shown in Figure 2.3.
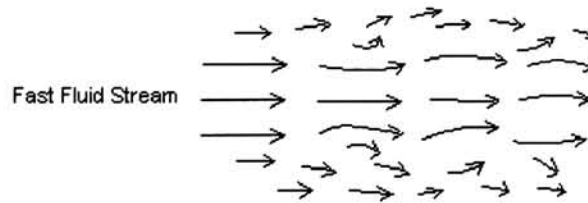
Figure 2.3. Velocity gradients between fast and slow moving fluid streams

Third, fluid flow past a sharp angularity can lead to internal turbulent flow. This causes separation of the flow and eddies to set-up in the wake region. This disturbs the flow and induces fluctuations of the velocity components in time.
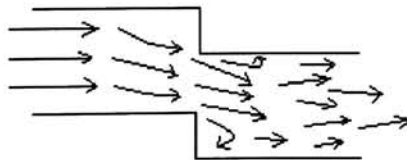
Figure 2.4. Fluid flow past a sharp angularity or corner

The above situations induce disturbances and instability into the fluid flow. This can ultimately generate turbulent fluid flow and aid in the atomization process. Due to this fact, these generation mechanisms were used in the design of the add-on nozzles. Geometries were created to separate the flow and create regions of vorticity and rotation. These regions hold energy-containing turbulent eddies of various sizes that can ultimately be related to the atomization process and resulting spray distribution.

2.5 Turbulence Modeling

Turbulent flows are relatively easy to describe. However, the analysis and modeling of the turbulent flow situation is a bit more difficult. Any fluid flow is regulated by three governing equations. These consist of the continuity equation (conservation of mass), the Navier-Stokes equations (Newton's second law), and the energy equation. The postulations involved in the derivation of these equations make no mention about the exclusion of turbulent flows. Therefore, they must be valid for the turbulent flow condition. One can attempt to solve these equations, numerically, for instantaneous quantities from the given boundary conditions. However, this isn't a practical alternative as far as memory and computing time is concerned. A more practical approach to describing turbulent flow is to model averaged turbulent transport quantities because the turbulent flow properties fluctuate and vary in time.[49] The time averaged continuity and Navier-Stokes equations are as follows:

$$\frac{\partial \bar{u}_i}{\partial x_i} = 0 \qquad (2.1)$$

$$\rho \frac{D\bar{u}_i}{Dt} = \rho \bar{g}_i - \frac{\partial \bar{P}}{\partial x_i} + \frac{\partial \bar{\tau}_{ij}}{\partial x_j} + \frac{\partial \bar{\tau}'_{ij}}{\partial x_j} \qquad (2.2)$$

where, ρ is the fluid density, $\bar{u}$ is the mean velocity component, g is the gravitational acceleration, $\bar{P}$ is the mean pressure term, $\bar{\tau}_{ij} = \mu \left(\frac{\partial \bar{u}_i}{\partial x_j} + \frac{\partial \bar{u}_j}{\partial x_i} \right)$, $\bar{\tau}'_{ij} = -\rho \overline{u'_i u'_j}$ (Reynolds Stress), μ is the fluid viscosity, u' is the fluctuating component of velocity, and the instantaneous velocity $u = \bar{u} + u'$.

In the averaging of the governing equations, fluctuating properties enter the picture (i.e. u'). We don't know their magnitudes so we must model these quantities with ones we can determine. This problem is called turbulence closure. Additional equations for closure are proposed on the premise that quantities such as turbulent kinetic energy, eddy size, and turbulent stress are transported by turbulent motion. Thus, additional differential equations are obtained from their equations of motion.[50] These equations, together with the time-averaged governing equations, called Reynolds time-averaged equations, are solved numerically. So, by the term turbulence model, one means a set of equations, when solved with the mean flow equations, allows calculation of relevant correlations and, hence, helps in simulating the behavior of real fluids.[50]

There are certain general postulations involved in turbulence modeling. Chen and Jaw[49] proposed the following: First, the Reynolds averaged Navier-Stokes equations can properly describe the turbulent mean motion and turbulent transport properties. Instantaneous fluid motions are averaged and detailed information about fluid motions is lost. A model is required to recover the lost information. Second, diffusion of turbulent transport properties is proportional to the gradient of transport properties. Third, small turbulent eddies are isotropic (non-direction dependent). Fourth, turbulent transport quantities are local functions of Reynolds stress, turbulent kinetic energy, rate of dissipation of turbulent kinetic energy, mean flow variables, and thermodynamic variables. Fifth, modeled turbulent phenomena must be consistent in symmetry, invariance, permutation, and physical observations. Sixth, turbulent phenomena can be characterized by one turbulent scale (either velocity (u), length (l), or time (t)) on the basis of turbulent kinetic energy (k) and its rate of dissipation (ε); $u=k^{1/2}$, $l=k^{3/2}/\varepsilon$, $t=k/\varepsilon$. And last, all turbulence model constants require experimental calibration and determination. For a turbulence model to be complete, the model constants should be unique and valid for any turbulent flow geometry and conditions. At present, no such turbulence model is available. Therefore many variations on turbulence models exist to account for many different situations.

The classification of turbulence models is quite simple. They are classified by the number of differential equations used in addition to the Reynolds averaged governing equations. They consist of zero-equation, one-equation, and two-equation models. Accuracy

increases with additional equations but the computational time is also increased. For the purposes of this investigation the standard k-ε model was chosen.

2.5.1 Standard k-ε Turbulence Model

This model falls under the category of two equation models. It uses two additional differential equations for the transport of turbulent kinetic energy, k, and its dissipation rate, ε. The transport of turbulent kinetic energy is defined as

$$\frac{Dk}{Dt} = \frac{\partial}{\partial x_l}\left(C_k\frac{k^2}{\varepsilon}\frac{\partial k}{\partial x_l} + v\frac{\partial k}{\partial x_l}\right) - \overline{u_i u_i}\frac{\partial \overline{u}_i}{\partial x_l} - \varepsilon \qquad (2.3)$$

where, $k = \frac{1}{2}\left(\overline{u'u'} + \overline{v'v'} + \overline{w'w'}\right)$, u', v', and w' are the fluctuating velocity components,

$\varepsilon = v\overline{\frac{\partial u_i'}{\partial x_j}\frac{\partial u_i'}{\partial x_i}}$, $v_t = C_\mu\frac{k^2}{\varepsilon}$, and $C_k = 0.09$ to 0.11.

The transport of the turbulent kinetic energy dissipation rate is given as

$$\frac{D\varepsilon}{Dt} = \frac{\partial}{\partial x_l}\left[\left(C_\varepsilon\frac{k^2}{\varepsilon} + v\right)\frac{\partial \varepsilon}{\partial x_l}\right] - C_{\varepsilon 1}\frac{\varepsilon}{k}\overline{u_i u_l}\frac{\partial \overline{u}_i}{\partial x_l} - C_{\varepsilon 2}\frac{\varepsilon^2}{k} \qquad (2.4)$$

where, $C_\varepsilon = 0.07$, $C_{\varepsilon 1} = 1.45$, and $C_{\varepsilon 2} = 1.92$.

This model has proven to be relatively accurate for the solution of certain general turbulent flows. It's superior to one-equation models and doesn't require a lot of computational time. It does however have certain limitations. It is only valid for fully turbulent flows and assumes the same eddy viscosity for all the Reynolds stresses. Also, the model is not valid in the region of the wall boundary layer where molecular and turbulence effects are of comparable magnitude.[51] Due to this fact, the model uses a wall function representation of the boundary layer behavior. There are certain assumptions based on this wall function representation[51]. First, variations in velocity and other properties are

predominantly normal to the wall, leading to one-dimensional behavior. Second, effects of pressure gradients and body forces are negligibly small, leading to uniform shear stress in the layer. Third, shear stress and velocity vectors are aligned and unidirectional throughout the layer. Fourth, a balance exists between turbulent energy production and its dissipation. And last, there is a linear variation of the turbulence length scale.

The standard k-ε model was chosen for this investigation in order to remain consistent with the theory behind the Huh Atomization Model[5]. The equations in this model were numerically solved with the mean flow equations for given nozzle geometries using a commercially available CFD software package (Fluent). The turbulent quantities output from Equations 2.3 and 2.4, namely k and ε, were input to the Huh Atomization Model[5] to relate the turbulent flow variables at the nozzle exit to a resulting secondary drop size distribution.

Chapter 3-Atomization Process

3.1 Introduction

Atomization is the process by which a volume of liquid is converted into smaller particles or droplets. It occurs when internal and external applied forces tend to disrupt the consolidating effects of surface tension. Breakup of the liquid transpires when these applied disruptive forces overcome the action of surface tension. In essence atomization is a growth disturbance process. External forces applied to an emerging stream of liquid (either a jet or sheet) tend to produce disturbances on the surface of the stream. Ultimately, it is the growth of such wavelike disturbances that leads to disintegration of the stream into droplets and then to a spray.

In a pMDI, a number of factors influence the atomization of the formulation. They include volatilization (flashing) of propellant, formulation properties, flow passage geometry, and the turbulence characteristics at the nozzle exit. No single atomization model has been developed to account for all of these factors. Models have been developed to account for the flashing of the propellant as the primary atomization mechanism.[45,46] This study was concerned with the effects of turbulence so, the Huh Atomization Model[5] was used to predict the droplet size distribution resulting from certain nozzle exit conditions. This model considers both turbulence and wave growth as important processes in atomization. The general atomization process, certain atomizers, and atomization models are considered in this chapter.

3.2 General Atomization Process

The atomization process is affected by many different factors. Issues ranging from atomizer geometry to the ambient conditions into which the flow is injected eventually determine the resulting spray characteristics.

Atomizer geometry and size greatly impact atomization. The final drop diameter achieved for a certain atomizer is almost always related to the square root of a certain critical dimension associated with the atomizer. This critical diameter or dimension could be the diameter of the discharge orifice, as in a plain orifice pressure atomizer, or the thickness of

the emerging liquid sheet, as in a pressure swirl atomizer. Also, the atomizer internal geometry has a large influence on the turbulent flow conditions at the nozzle exit.

Liquid Properties such as surface tension and viscosity also affect the spray production process. Surface tension tends to pull the liquid together to resist the action of disruptive forces. Viscosity tends to affect nozzle flow rate and spray pattern. It acts as a stabilizing force that opposes changes in geometry. Highly viscous fluids tend to hinder the onset of turbulent flow and the development of natural instabilities associated with this turbulence.

The velocity of the emerging fluid has a profound influence on the spray characteristics. Ultimately turbulence is a desired factor and leads to better atomization. Turbulent velocity profiles produce higher shear stress at the walls of the atomizer along with larger components of radial velocity. Both of these serve to disrupt surface tension and lead to a finer spray. As we will see later, the development of the proper turbulent conditions is crucial to producing a finer spray.

The ambient conditions into which a spray is injected can greatly affect the atomization process. The pressure, density, and temperature of the external gas all can lead to changes in aerodynamic and other external forces on the droplets. This can lead to alterations in median drop size along with other spray characteristics.

3.2.1 Mechanisms of Atomization

Atomization involves the conversion of a bulk liquid into a distribution of small drops. Most often, a stream of liquid emerges from an atomizer in the form of a liquid jet or sheet. In the case of a pMDI, the emerging flow is in the form of a jet. This section is devoted to the various mechanisms used to account for the manner in which these jets are disintegrated into droplets as described by Lefebvre[52].

Disintegration of Liquid Jets

As a jet emerges from a nozzle as a continuous body, the interactions between cohesive and disruptive forces give rise to oscillations and disturbances on the jet surface. The oscillations and disturbances lead to the breakup of the jet. As the Reynolds number increases we see an increase in disturbances due to an increase in the aerodynamic forces or dynamic pressure from the ambient air. This leads to a classification of different modes of disintegration based

on the Ohnesorge number vs. the Reynolds number. The Ohnesorge number is a dimensionless group obtained by dividing the square root of the Weber number by the Reynolds number and it is a measure of jet stability. Ohnesorge[53] proposed an early classification of the different modes. A more recent study by Reitz[54] attempted to solve some of the uncertainties surrounding the Ohnesorge chart. Reitz came up with four regimes of breakup encountered as the liquid jet velocity increases, as shown in Figure 3.1.
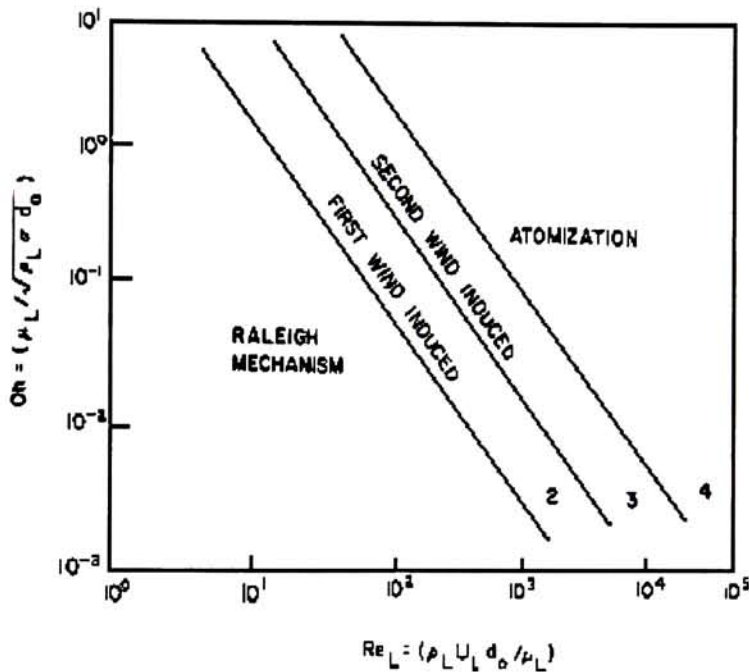
Figure 3.1. Jet breakup modes[52]

The first is the Rayleigh jet breakup regime. It is caused by the growth of axisymmetric oscillations of the jet surface induced by surface tension. The drop diameters exceed the jet diameter in this region. Second is the First Wind Induced Breakup region. In this region, the surface tension is now augmented by the relative velocity between the jet and ambient gas. Dynamic pressure is now a factor and the final drop diameter is similar to the jet diameter. Third is Second Wind Induced Breakup. In this region, drops are produced by the unstable growth of surface waves on the jet surface caused by the dynamic pressure of the ambient air. The growth is once again opposed by surface tension and the drop size is much less than the initial jet diameter. The last regime of breakup is atomization. In this region, the jet disrupts completely at the nozzle exit. The drop diameters are much, much less than the jet diameter and the predominant mechanism of breakup is unknown.

Influence of Jet Velocity Profile on Breakup

For a given nozzle, the state of flow in the nozzle is defined by the flow upstream of the orifice and by disturbances produced in the approach passages. The nature of the flow is characterized by the Reynolds number and has a profound effect on the breakup of the jet.

Laminar Flow is a very layered flow in which the liquid particles flow in streams parallel to the axis of the tube. The velocity profile of the jet, immediately downstream of the orifice, varies in a parabolic manner. Further downstream, momentum transfer occurs between the layers of the flow and a process of velocity profile relaxation occurs. This leads to a flatter profile with the same mean velocity as the original. Air friction and surface tension forces combine to create irregularities and lead to disintegration.

Semi-turbulent Flow is characterized by an annulus of laminar flow surrounding a turbulent core. Initially particles of the core are prevented from reaching the surface of the jet. Further downstream, the profile relaxes. This brings liquid particles with radial components of velocity to the surface. These liquid particles lead to disturbances and disintegration of the jet.

Turbulent and high velocity flow is characterized by high momentum, random flow with large radial components of velocity. These large components, along with higher shear stress and aerodynamic forces, produce disturbances that lead to breakup. The exact turbulent flow condition is described by k and ε and these turbulent quantities dictate the spray characteristics described by the Huh Atomization Model[5].

Stability Curve

The stability curve, shown in Figure 3.2, illustrates the relationship between the jet velocity profile and the length of the continuous portion of the jet. This is known as the breakup length and it is measured from the nozzle to the point of drop formation.
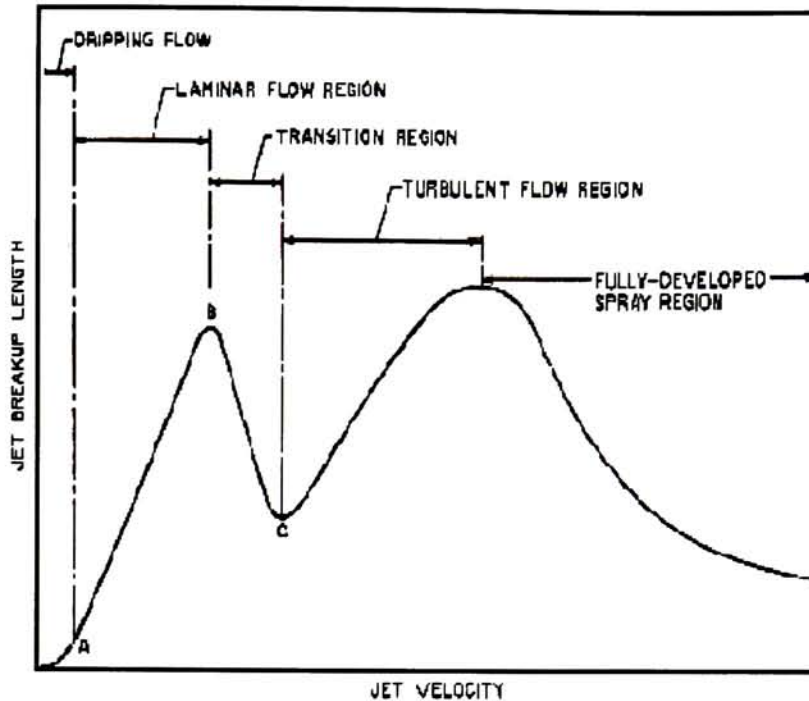
Figure 3.2. Jet stability curve[52]

As the jet velocity is increased the flow regime changes from dripping to laminar to turbulent flow. The jet breakup length increases as the flow changes from dripping to laminar. As the jet transitions from laminar to turbulent the breakup length tends to decrease. The breakup length again increases as the jet velocity increases in the turbulent flow region. Further increases in the jet velocity lead to a maximum breakup length after which the spray becomes fully developed.

Breakup of Drops

The breakup of a single liquid drop in air is the result of its aerodynamic interaction with the air. In general the deformation of a drop is determined by the ratio of aerodynamic forces to surface tension forces. This ratio is known as the Weber number. Larger deforming forces correspond to a higher Weber number and lead to greater breakup. This breakup can occur in stagnant air as well as in flowing air.

Breakup in stagnant air

This breakup occurs as a result of interaction between a falling drop and the surrounding air. Two things can occur under the action of aerodynamic forces. First, equilibrium between

aerodynamic and internal forces can be reached. The critical Weber number characterizes this point when drag is equal to surface tension. This is a stable condition and the drop will remain stable as long as a change in air pressure on the surface can be compensated by a corresponding change in the pressure due to surface tension. If the combination of surface tension and aerodynamic forces remains constant stability will be maintained. Second, aerodynamic forces deform the drop until breakup occurs. Breakup will occur if a change in pressure due to aerodynamic forces is not compensated by the change in the surface tension forces. Drops will breakup until they reach a critical stable size.

Breakup in flowing air

This breakup occurs as a result of the interaction between a droplet and a flowing air stream. This breakup can occur in three ways. First, the drop if flattened by aerodynamic forces into an ablate ellipsoid. This is called lenticular deformation and it is produced by parallel and rotation flows. Second, the drop is elongated to form a ligament. This is known as cigar deformation and it is produced by plane hyperbolic and Couette flows. And last, local deformations on drop surface create bulges and protuberances, which form smaller drops. This deformation is due to irregular flow patterns.

3.3 Atomizers

Sprays may be produced in a variety of ways. Depending on the applications, different types of atomizers may be better suited to produce the desired spray characteristics. Atomizers are characterized by the method in which they produce a spray, and the various types are summarized according to Lefebvre[52] as follows.

3.3.1 Pressure Atomizers

As their name suggests, pressure atomizers rely on the conversion of pressure into kinetic energy to achieve a relatively high velocity flow. It is this high relative velocity between the liquid and the surrounding gas that leads to atomization.

In a Plain Orifice Pressure Atomizer, liquid is passed through a small circular orifice to produce atomization. A pMDI is essentially a plain orifice pressure atomizer. The high-pressure propellant provides the energy to disintegrate the flow through the plain circular orifice. Atomization is promoted by an increase in flow velocity, which leads to turbulence

and increased aerodynamic drag. In essence, the flow in the Plain Orifice Pressure Atomizer is similar to the flow in a pipe, thus it is characterized by the Reynolds number. The flow number is the ratio of the nozzle throughput to the square root of the injection pressure differential. The spray is more rapidly dispersed at high Reynolds number due to transition from laminar to turbulent flow. The proper turbulent flow condition leads to greater atomization. The discharge coefficient is often used to characterize flow on exit from the atomizer. It is defined as the ratio of the actual flow rate to the theoretical value. The discharge coefficient is influenced by many factors including Reynolds Number, length to diameter ratio of the orifice, injection pressure, ambient pressure, inlet chamfer, and cavitation.

In the Simplex or Pressure Swirl Atomizer, a swirling motion is imparted to the liquid so that, under the action of centrifugal force, it spreads out in the form of a conical sheet as soon as it leaves the orifice. There are two types of simplex nozzles consisting of the solid cone and the hollow cone. The solid cone forms a spray comprised of drops distributed uniformly throughout its volume. The hollow cone issues drops concentrated at the outer edge of the spray pattern. Development of the spray in the simplex atomizer passes through several stages as liquid injection pressure is increased from zero. The simplex is able to achieve wider cone angles than the plain orifice and can produce good atomization over wide ranges with the use of wide range nozzles.

A Duplex Pressure Atomizer is similar to the simplex, but its swirl chamber employs two sets of tangential ports. The primary port is utilized for low flows where the main or secondary passage is used for larger flows.

The Dual Orifice Pressure Atomizer essentially comprises two simplex nozzles that are fitted concentrically on the atomizer. The primary nozzle is located on the inside with the secondary on the outside. The primary and secondary nozzles are situated such that the individual sprays don't interfere with each other.

The Spill Return Pressure Atomizer is basically a modified simplex atomizer. The rear wall of the swirl chamber contains a passage through which liquid can be "spilled" away from the atomizer. The atomizer uses a relatively high constant pressure to ensure adequate swirl and efficient atomization at low flow rates.

3.3.2 Rotary Atomizers

In this type of atomizer, liquid is fed onto a rotating surface where it spreads out fairly uniformly under the action of centrifugal forces. The rotating surface may take the form of a flat disk, vaned disk, cup, or slotted wheel. There are several mechanisms involved in this type of atomization. Ligament formation at the rim leads to formation of discrete drops. An increase in flow rate leads to the formation of a sheet at the rim that disintegrates into drops. Atomization quality is improved with an increase in RPM, a decrease in liquid flow rate or viscosity, and serration of the outer edge.

3.3.3 Air-Assist Atomizers

As their name also suggests, Air-Assist Atomizers use flowing air to aid in the disintegration of a liquid jet or sheet. These atomizers are comparable to jet nebulizers. Some of these atomizers use air to supplement the atomization process at low flow rates, while others require air to achieve the atomization process at any flow rate.

Air-Assist Atomizers are comprised of Internal and External Mixing, the Parker-Hamifin and Lezzon Nozzles, and the Y-Jet types. The Internal Mixing Air-Assist Atomizer is suitable for highly viscous liquids and uses airflow to assist atomization at low flow rates. The spray cone angle is minimum for maximum airflow and widens as the airflow rate decreases. The External Mixing atomizer also uses air to supplement atomization at low flow rates and a constant spray cone angle is achievable at all flow rates. The Parker-Hamifin Nozzle uses inner and outer airstreams to achieve a shearing action on an annular liquid sheet at the nozzle tip. Airflow is necessary for atomization in this atomizer. In the Lezzon Nozzle, inner and outer airflows are used to achieve a shearing action. The difference between this and the Parker-Hamifin Nozzle is the fact that air and liquid interact before issuing from the nozzle. The Y-Jet atomizer utilizes a number of jets arranged in an annular fashion to provide a hollow conical spray.

3.3.4 Airblast Atomizers

In principle, these atomizers are the same as the Air-Assist class. However, a main difference lies in the quantity and velocity of air supplied. Air-Assist Atomizers use small

quantities of high velocity air while Airblast Atomizers use much larger amounts of air for atomization.

The three categories of Airblast Atomizers include the Prefilming, Piloted, and Plain-jet types. The Prefilming-Airblast Atomizer achieves atomization by subjecting a thin liquid sheet to high velocity air. The Piloted or Hybrid Airblast Atomizer combines the Prefilming type with the action of a simplex nozzle. This was designed to overcome poor atomization at low air velocities. The Plain Jet Airblast Atomizer utilizes liquid injected into the air stream in one or more discrete jets to produce an atomized spray.

3.3.5 Other Atomizers

Three other atomizer types exist. They consist of Effervescent, Electrostatic, and Ultrasonic Atomizers.

In Effervescent Atomizers, the air or gas used in atomization is introduced directly into the bulk liquid at a point upstream of the nozzle. This produces good atomization at low injection pressures and flow rates. Electrostatic Atomizers use the mutual repulsion of like charges that have accumulated on the surface of the liquid. These charges produce an electrical pressure, which acts to disrupt surface tension. In the Ultrasonic Atomizer (Nebulizer), the liquid is introduced onto a rapidly vibrating surface leading to wave patterns formed on the liquid. Atomization occurs when the amplitude of the waves become high enough to become unstable and collapse. This leads to formation of a mist of small drops to be ejected from the surface. Low flow rates are required for atomization and droplet sizes are sufficiently small for inhalation.

3.4 Atomization Models

Atomization models are developed according to the type of atomizer used to produce the spray. The models contain empirical equations that express the relationship between the mean drop size in a spray and the variables of liquid properties, gas properties, flow conditions, and atomizer dimensions.[52]

This study is concerned with the spray issued from the pMDI. A pMDI is essentially a plain orifice pressure atomizer. Within the scope of the atomization process in this device lies the influence of the turbulent flow condition. Changes in the turbulent flow condition

due to alterations in nozzle geometry can greatly affect the spray distribution. The Huh Atomization Model[5] was chosen to predict the spray distribution resulting from certain nozzle geometries because it links turbulent flow characteristics at the nozzle exit to the exterior atomization process.

3.4.1 Huh Atomization Model[5]

The Huh Atomization Model[5] considers the two independent mechanisms of turbulence and wave growth in an attempt to provide a logical framework for coupling the flow inside the nozzle to the exterior spray production process.[5] The turbulent fluctuating motions developed within the nozzle provide initial perturbations on the ensuing jet surface. These perturbations undergo a wave growth process due to interaction with the surrounding air and cause the jet to breakup into a spray.

In this model, the spray computation is divided into two groups, primary and secondary parcels. The primary parcel is the one injected from the nozzle, whereas the secondary parcel is generated from the primary one.[5] Primary droplets ultimately breakup entirely into secondary ones. Thus, the probability density function (PDF) for the diameter of the secondary droplet (p(x)) will be able to adequately represent the characteristics of the spray at a chosen time. p(x) is proportional to the turbulence energy spectrum and inversely proportional to the atomization time scale given by Huh et al[5] as

$$p(x) = C \frac{\phi(x)}{\tau_A(x)} \qquad (3.1)$$

where $\phi(x)$ is the turbulence energy spectrum, $\tau_A(x)$ is the atomization time scale, and C is a constant.

The constant C is determined by the normalization condition given by

$$\int_0^\infty p(x)dx = 1.0 \qquad (3.2)$$

The turbulence energy spectrum is given as

$$\phi(x) = C \frac{(\lambda/\lambda_e)^2}{\left[1 + (\lambda/\lambda_e)^2\right]^{11/6}} \qquad (3.3)$$

where, the wave number λ, is the inverse of the drop diameter, x. The wave number associated with the maximum energy in the turbulent energy spectrum, λ_e is obtained from

$$\lambda_e = \frac{1}{L_e} \qquad (3.4)$$

where L_e is the size of the eddies with the maximum energy in the turbulence energy spectrum given as

$$L_e = \frac{L_t}{0.75} \qquad (3.5)$$

L_t is the turbulence length scale and is expressed as

$$L_t(t) = L_t^o \left[1 + \frac{0.0828t}{\tau_t^o}\right]^{0.457} \qquad (3.6)$$

where t is the time since injection from the nozzle and L_t^o and τ_t^o are the initial turbulence length and time scales, respectively, defined as

$$L_t^o = C_\mu \frac{k_{avg}^{3/2}}{\varepsilon_{avg}} \qquad (3.7)$$

$$\tau_t^o = C_\mu \frac{k_{avg}}{\varepsilon_{avg}} \quad (3.8)$$

where k_{avg} and ε_{avg} are the average turbulent kinetic energy and energy dissipation rate, respectively. They are calculated at the nozzle exit from the standard k-ε model for turbulent fluid flow. C_μ is a constant given in this model for turbulence and is equal to 0.09. Combining equations 3.4, 3.5, 3.6, 3.7, and 3.8 yields the following equation for λ_e.

$$\lambda_e = \frac{\dfrac{0.75}{C_\mu} \varepsilon_{avg}}{k_{avg}^{3/2} \left[\dfrac{k_{avg} + \dfrac{0.0828}{C_\mu} \varepsilon_{avg} t}{k_{avg}} \right]^{0.457}} \quad (3.9)$$

Substituting Equation 3.9 into Equation 3.3 and noting that $\lambda=1/x$, the turbulence energy spectrum becomes

$$\phi(x) = 1.78 CC_\mu^2 k_{avg}^{2.086} \varepsilon_{avg}^{5/3} x^{5/3} \left(k_{avg} + \frac{0.0828}{C_\mu} \varepsilon_{avg} t \right)^{0.914} \left[\varepsilon_{avg}^2 x^2 + 1.78 C_\mu^2 k_{avg}^{2.086} \left(k_{avg} + \frac{0.0828}{C_\mu} \varepsilon_{avg} t \right)^{0.914} \right]^{-11/6}$$

(3.10)

Referring back to Equation 3.1, τ_A was defined as the atomization time scale. It is expressed as a linear sum of the turbulence and wave growth time scales as follows:

$$\tau_A = 1.2\tau_t + 0.5\tau_w \quad (3.11)$$

τ_t is the turbulence time scale expressed as

$$\tau_t = \tau_t^o + 0.0828t \qquad (3.12)$$

where t is the time. τ_w is the wave growth time scale given as

$$\tau_w = \cfrac{1}{\sqrt{\cfrac{\rho_g}{\rho_f}\cfrac{U}{L_w}}} \qquad (3.13)$$

where ρ_g is the gas density, ρ_f is the density of the fluid to be atomized, U is the mean injection velocity from the nozzle, and L_w is the wave growth length scale.

L_w is equal to twice the atomization length scale, L_A. It is assumed that the length scale of turbulence is the dominant length scale of atomization so that $L_A = 2L_t$. Thus,

$$L_w = 4L_t \qquad (3.14)$$

Combining Equations 3.6, 3.7, 3.8, and 3.14, L_w becomes

$$L_w(t) = 4C_\mu \frac{k_{avg}^{3/2}}{\varepsilon_{avg}}\left[1 + \frac{0.0828t}{C_\mu \dfrac{k_{avg}}{\varepsilon_{avg}}}\right]^{0.457} \qquad (3.15)$$

Uniting Equations 3.8, 3.11, 3.12, 3.13, and 3.15, the atomization time scale becomes

$$\tau_A = 1.2C_\mu \frac{k_{avg}}{\varepsilon_{avg}} + 0.09936t + \frac{C_\mu^{0.2715}\rho_f^{1/2}k_{avg}^{0.5215}\left(C_\mu k_{avg} + 0.0828t\varepsilon_{avg}\right)^{0.2285}}{\rho_g^{1/2}U^{1/2}\varepsilon_{avg}^{1/2}} \qquad (3.16)$$

Using Equations 3.1, 3.2, 3.10, and 3.16 the probability density function for the secondary drop size distribution can be determined. The variables required to determine the PDF are k_{avg}, ε_{avg}, U, ρ_g, ρ_f, and t. k_{avg} and ε_{avg} are determined through the application of the standard k-ε turbulence model to the given nozzle geometry using a commercially available CFD package. U was determined through the application of the conservation of mass using the flow rate for the standard inhaler. ρ_g and ρ_f are properties of given fluids; in this case air and water were used. The time, t, was calculated from U and a given distance from the nozzle exit. The distance chosen was approximately three inches from the nozzle exit. This length was picked to simulate the time when the aerosol would reach the back of the throat (in actuality, any time could have been chosen to compare the secondary droplet distributions from the corresponding nozzles as long as it remained consistent throughout the analysis).

This model was developed on the basis that atomization is a combined process of turbulent fluctuating motions producing initial perturbations and subsequent breakup by wave growth. These concepts concur with the reasoning this study was based on and thus this model was chosen to predict droplet size distributions from turbulence conditions on exit from the resulting nozzle. These results are described later in this report in Chapter 4.

### 3.4.2 Huh Atomization Model[5] Analysis

The goal of this study was to improve the spray characteristic of the pMDI through the use of an add-on turbulence generating nozzle. An analysis of the Huh Atomization Model[5] was needed to determine the range of exit turbulence parameters that lead to a reduction in the median secondary drop size.

The PDF for the secondary drop size distribution is directly related to the turbulence energy spectrum and inversely related to the atomization time scale, as seen from Equation 3.1. In actuality, the atomization time scale is constant for a given k, ε, U, and time so the PDF is directly dependent on the turbulence energy spectrum. One of the characteristics of turbulent flow is the presence of eddies, or rotational fluid chunks that are transported with the flow. These eddies come in various sizes from small to large. The turbulence energy spectrum is a measure of the distribution of turbulent energy within the eddy system of the flow field. It describes how much energy is associated with eddies of varying sizes and holds the key to the prediction of the PDF. If we refer back to Equation 3.3, we see that the

turbulence energy spectrum ($\phi(x)$) is dependent on λ and λ_e. If we impose the definitions of λ and λ_e, $\phi(x)$ becomes,

$$\phi(x) = C \frac{(L_e/x)^2}{\left[1 + (L_e/x)^2\right]^{11/6}} \qquad (3.17)$$

Equation 3.17 was derived to show that a decrease in L_e would shift both $\phi(x)$ and $p(x)$ toward the left thus decreasing the median droplet size. This is illustrated in Figure 3.3.
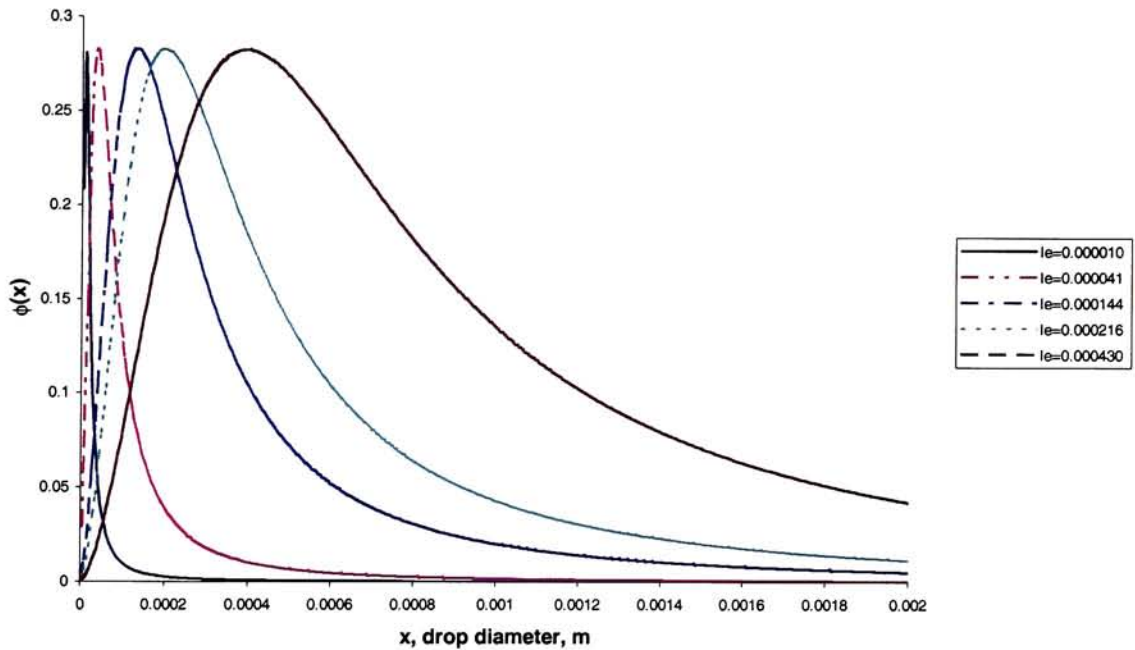

Figure 3.3. Turbulence energy spectrum vs. drop diameter for decreasing L_e

L_e is the average length of the energy containing eddies and is directly related to the turbulence length scale (L_t) through Equation 3.5. So, a reduction in the turbulence length scale ultimately reduces the median droplet size. From equations 3.6, 3.7, and 3.8 we can see that L_t is related to k_{avg} and ε_{avg} as,

$$L_t(t) = C_\mu \frac{k_{avg}^{3/2}}{\varepsilon_{avg}} \left[1 + \frac{0.0828 t \varepsilon_{avg}}{C_\mu k_{avg}}\right]^{0.457} \qquad (3.18)$$

Figure 3.4 shows a plot of the turbulence length scale as a function of ε_{avg} for different k_{avg} values. C_μ and t are kept constant at 0.09 and 0.0045s respectively.
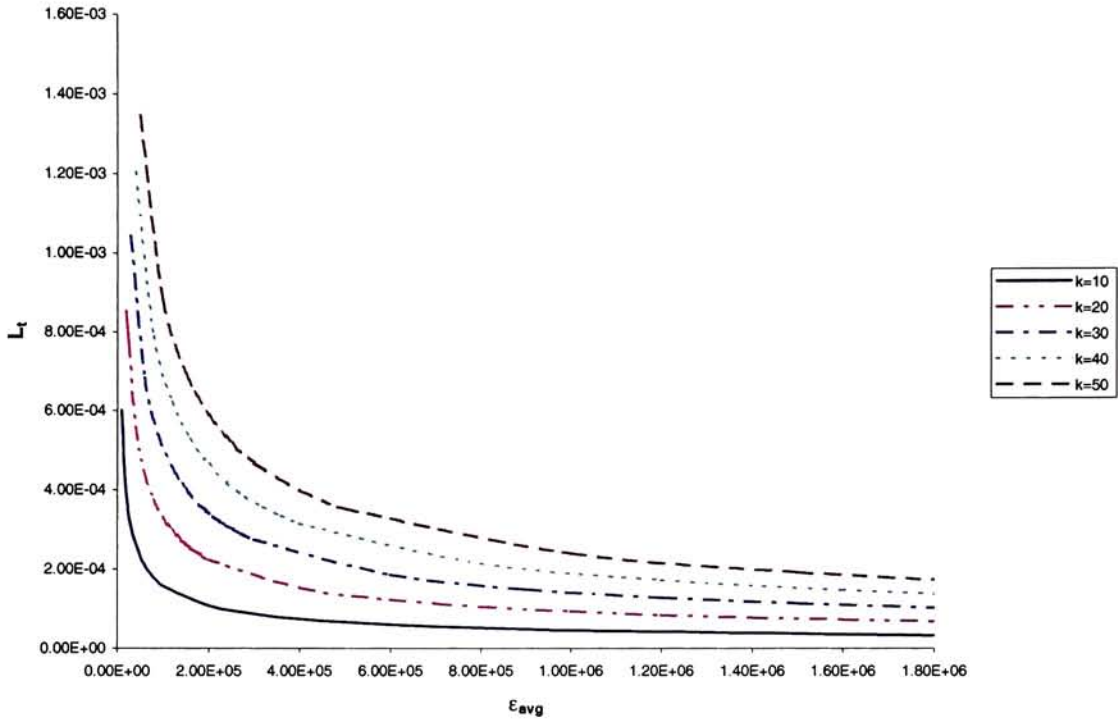
Figure 3.4. Turbulence length scale vs. average turbulent kinetic energy dissipation rate with average turbulent kinetic energy as a parameter

From Figure 3.4, we can see that a lower k_{avg} value with a higher ε_{avg} value leads to a lower turbulence length scale. A reduced value for L_t leads to a smaller L_e and a shift in the turbulence energy spectrum toward the origin, thus producing a lower median droplet size.

Figure 3.5 demonstrates that the median droplet size decreases as the $k_{avg}/\varepsilon_{avg}$ ratio decreases for decreasing values of k_{avg}. This reinforces the conclusions drawn from Figure 3.4.
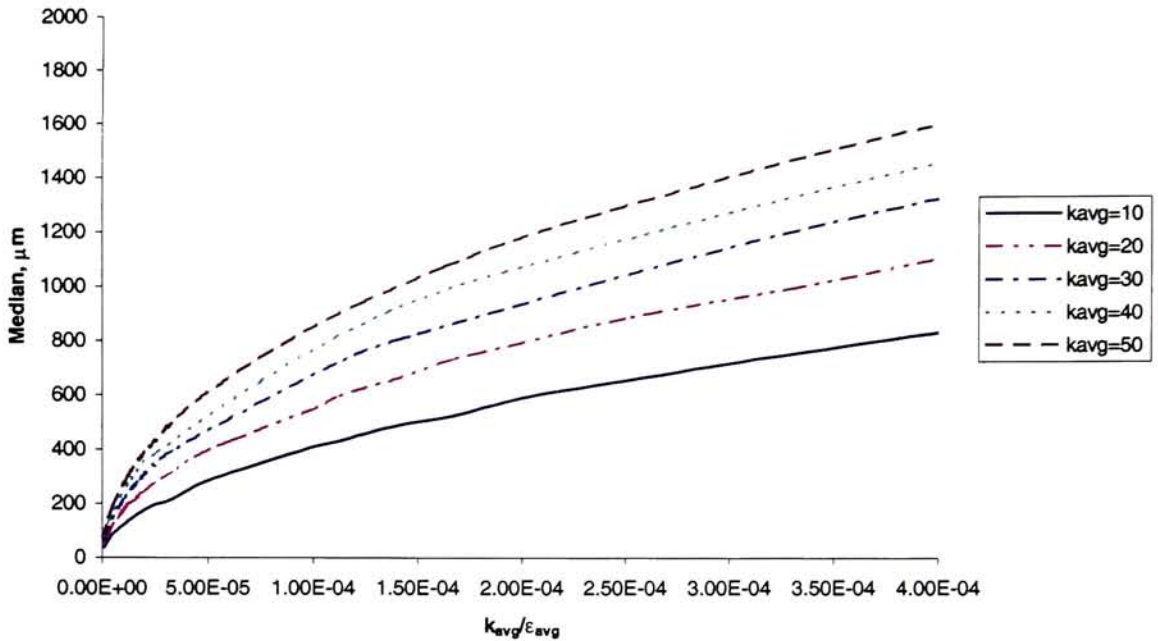
Figure 3.5. Median droplet size vs. $k_{avg}/\varepsilon_{avg}$ ratio with k_{avg} as a parameter

In conclusion, the above analysis shows that producing a low $k_{avg}/\varepsilon_{avg}$ ratio at a relatively low value of k_{avg} can reduce the median droplet size. In practical terms, increasing ε_{avg} for a constant value of k_{avg} produces a shift in the energy containing eddies from larger to smaller sizes. Smaller eddies are more efficient in dissipating energy than larger ones[50] so the turbulent kinetic energy is concentrated in eddies of smaller sizes, which ultimately produces a reduced median secondary droplet size.

Chapter 4-Modeling

4.1 Introduction

To improve upon the turbulence characteristics of the existing inhaler, the current flow passage was modeled and a baseline set for the median droplet size based on turbulence. The examination into the Huh Atomization Model[5], completed in section 3.4.2, confirmed that a low $k_{avg}/\varepsilon_{avg}$ ratio at a relatively low value of k_{avg} at the nozzle exit could reduce the median droplet size. Following this examination, new nozzles were designed in an effort to develop these proper turbulence conditions. The nozzle with the most potential was chosen and subsequently optimized to produce the lowest median secondary droplet size obtainable and thus the biggest improvement over the baseline value.

4.2 Baseline Model of Inhaler Internal Flow Passage

Dimensions of the inhaler actuator device were determined and used to create a three dimensional geometric model and mesh of the internal flow passage using Gambit, Fluent, Inc. The geometry dictated that the tetrahedral/hybrid mesh be used. The mesh was generated using an interval count method. This method divides all of the geometric entities of the model into the same number of intervals or elements in order to discretize the solution domain. The grid quality, namely the equiangle skew, was checked using the mesh check tool in Gambit, Fluent, Inc. This mesh was imported into Computational Fluid Dynamics Software (Fluent, Fluent, Inc.) where the turbulence model, boundary conditions, and fluid properties were assigned. As mentioned previously, the standard k-ε model was used for the turbulence model. A volumetric flow rate of 5.0e-06 m^3/s was used for all of the nozzles. This was calculated from a 100 μL output volume and 20 ms aerosol production time for the pMDI.[14] Using an inlet area of 2.138e-06 m^2, this led to a velocity inlet boundary condition of 2.338 m/s, based on mass conservation. The turbulent boundary conditions at the inlet were estimated using the turbulent intensity and length scale. The turbulent intensity, I is estimated using Reynolds number, R_e as,

$$I \cong 0.16 R_e^{-\frac{1}{8}} \quad (4.1)$$

where R_e is,

$$R_e = \frac{\rho_f U D}{\mu} \quad (4.2)$$

in which ρ_f is the fluid density, U is the mean velocity at the inlet, D is the inlet diameter, and μ is the fluid viscosity. Using ρ_f = 1000 kg/m3, U = 2.338 m/s, D = 0.00165 m, and μ = 0.001 Pa-s the Reynolds number at the inlet is 3857. This leads to an inlet turbulent intensity of 5.7%. The turbulent length scale, l is estimated as

$$l = 0.07 D \quad (4.3)$$

resulting in a turbulent length scale of 1.155e-04 m.

This investigation was concerned mainly with the comparison of the turbulent characteristics of the existing flow passage with that of new nozzles; so, water was chosen as the fluid to simulate the flow of the drug. It is assumed that the resulting relative improvement will not be changed for different fluid properties. A zero normal-gradient boundary condition was used at the nozzle exit for all of the flow properties except pressure. This condition is used when outlet conditions aren't known and want to be determined. Figure 4.1 illustrates the boundary conditions used in the inhaler baseline model.


Inlet B.C.'s
V=2.34 m/s (normal to boundary)
I=5.7 % (turbulent intensity)
l=1.155e-04 m (turbulent length scale)

Fluid Properties
ρ_f = 1000 kg/m3
μ = 0.001 Pa-s

Outlet B.C.'s
Outflow condition-assumes zero normal gradient for all flow properties except pressure (used when outlet conditions aren't known and want to be determined)
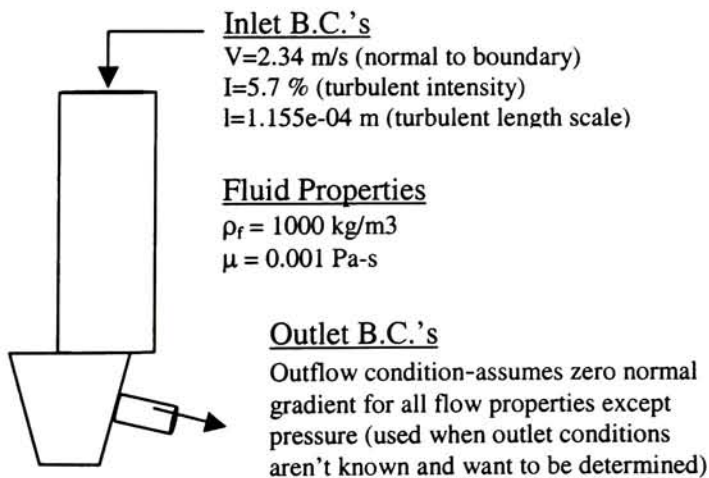
Figure 4.1. Schematic of baseline inhaler model boundary conditions

4.2.1 Baseline Model Results

The main results of this analysis include the turbulent kinetic energy (k), the turbulent kinetic energy dissipation rate (ε), and the velocity (u). The results of the computational flow analysis of the baseline model are shown as contour plots in Figures 4.2, 4.3, and 4.4.

Figure 4.2 shows the contours of k throughout the inhaler. The main point of interest is on exit from the nozzle.
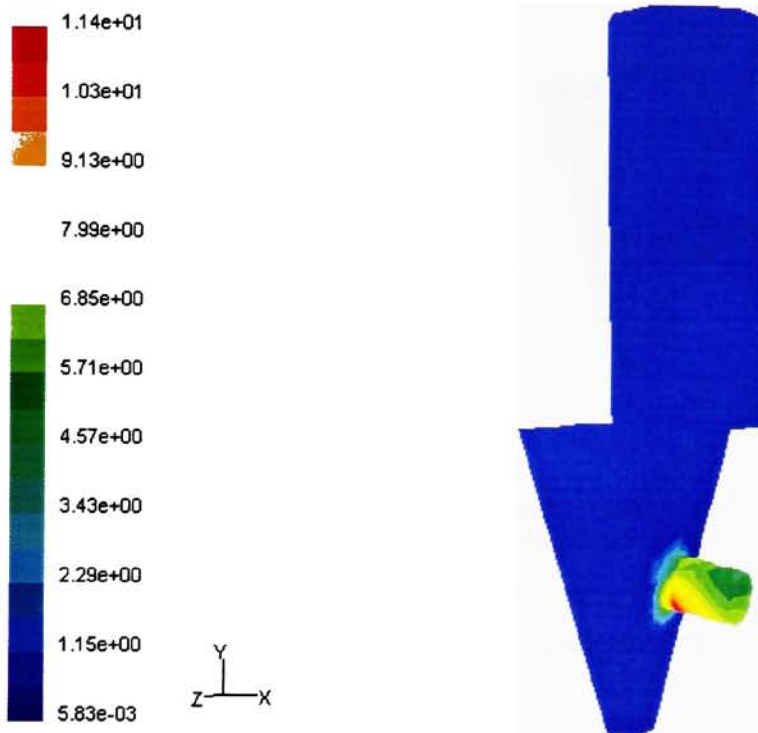
Figure 4.2. Inhaler internal flow passage-contours of turbulent kinetic energy, k_{avg}=5.8 m²/s²

An average value of k at the nozzle exit was needed to input into the Huh Atomization Model[5] to predict a median secondary droplet size. A vertex average was used to calculate this quantity. This type of average uses the values of k at the nodes on the exit face to determine the average. The results of this computation are k_{avg}=5.8 m²/s².

The contours of ε are shown if Figure 4.3. Again, the area of concern for this investigation is at the outflow location.
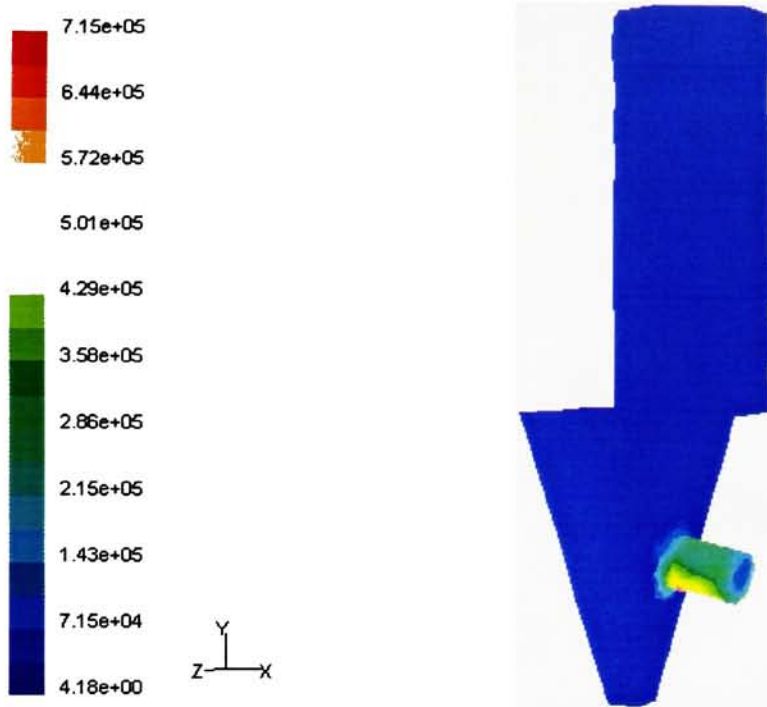
Figure 4.3. Inhaler internal flow passage-contours of turbulent kinetic energy dissipation rate, $\varepsilon_{avg}=7.0e+04$ m²/s³

An average value of ε at the nozzle exit was also needed to input into the Huh Atomization Model[5] to predict a median secondary droplet size. The results of this computation are $\varepsilon_{avg}=7.0e+04$ m²/s³.

The velocity contours were plotted in Figure 4.4. As a check to see that the results were close to what was expected, the mean velocity at the exit was calculated and compared to the computational result. The mean velocity with a nozzle exit diameter of 0.0006 m is expected to be around 17.7 m/s based on mass conservation. The computational result is approximately 17.8 m/s. This result agrees with the previous calculation.
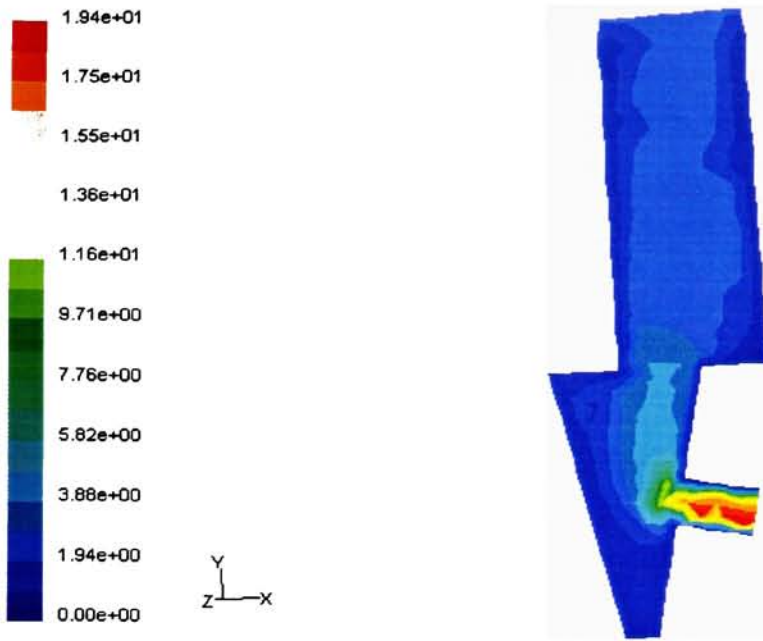
Figure 4.4. Inhaler internal flow passage-2D section of 3D velocity contours

The turbulence exit conditions of the nozzle were used to find the probability density function (PDF) and median secondary droplet size. The PDF for the secondary drop sizes was predicted from the Huh Atomization Model[5] for $k_{avg}=5.8$ m^2/s^2 and $\varepsilon_{avg}=7.0e+04$ m^2/s^3 and is shown in Figure 4.5.
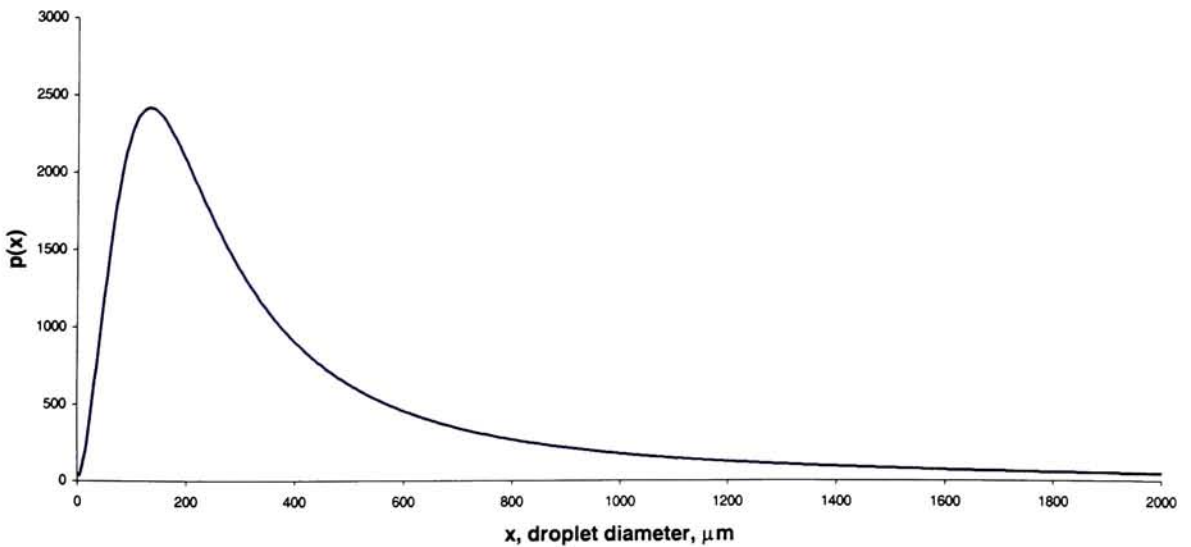
Figure 4.5. PDF for the baseline inhaler internal flow passage

The cumulative secondary drop size distribution, F(x) can be calculated from the PDF and this is shown in Figure 4.6.
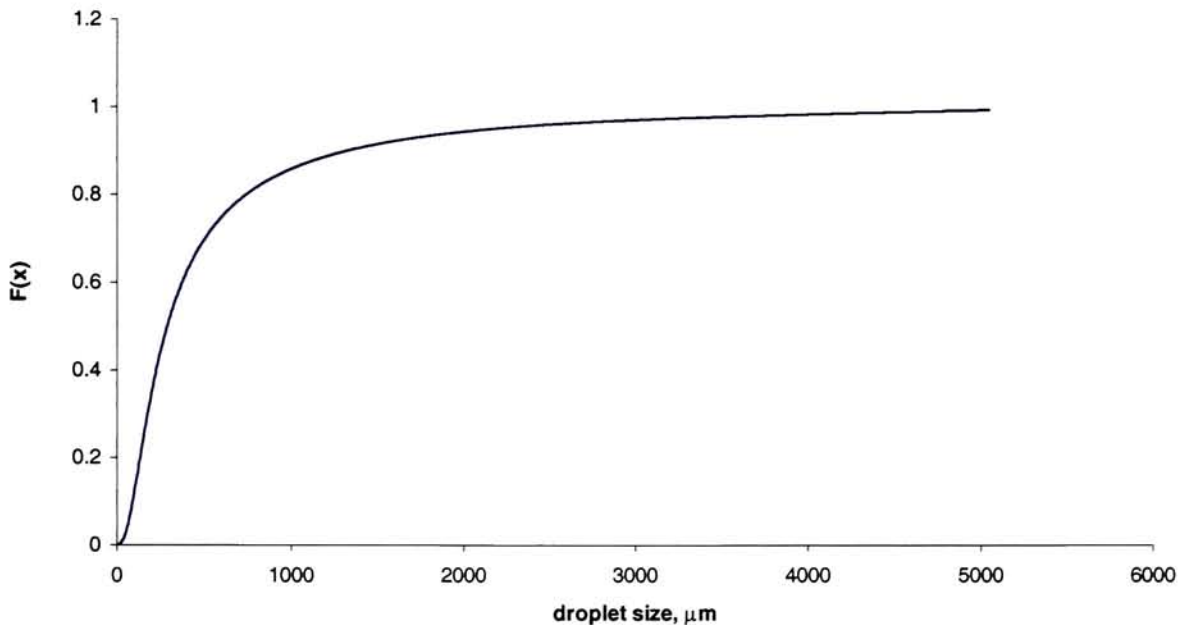
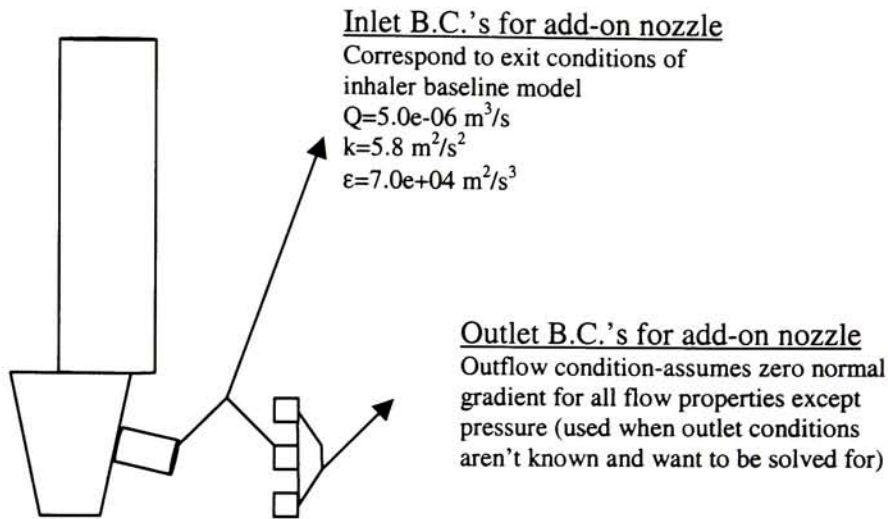**Figure 4.6. Cumulative secondary drop size distribution**

The area under the PDF is set equal to 1.0 through the use of the normalization constant (Equation 3.2) described in Section 3.4.1. It follows then that the median is the droplet diameter at which the area under the PDF is equal to 0.5. This is the same point at which the cumulative size distribution will be equal to 0.5. This value was found to be 290 μm for the baseline inhaler internal flow passage. It is important to note that this median droplet size is not the same as the median droplet size produced from an actual pMDI. As mentioned previously, the atomization process in the actual pMDI involves many mechanisms. In this case, we are just considering turbulence effects alone. The median value of the secondary droplet size at this location was chosen as a representative number for the spray from the baseline inhaler model based on turbulence exit conditions. In this investigation, we are making a comparative analysis between the baseline model and the baseline/add-on nozzle combination. This approach should be valid in showing relative differences between the two nozzle types.

4.3 Design of Add-on Nozzles

The add-on nozzles were designed with turbulence, simplicity, and the manufacturing process in mind. The manufacturing process, discussed in Appendix A, imposed certain restrictions on the nozzle dimensions including the nozzle thickness and the etch angles possible. The goal was to reduce the median secondary droplet size while maintaining an exit velocity similar to that of the current inhaler internal flow passages (approximately 17.8 m/s). Analysis of the Huh Atomization Model[5] (Section 3.4.2) showed that the turbulence exit conditions that produce a reduced median secondary droplet size are a low $k_{avg}/\varepsilon_{avg}$ ratio at a relatively low value of k_{avg}. It is very difficult to get a physical feel for exactly what geometric factors lead to these conditions. It is somewhat easier to get a feel for what factors lead to general internal turbulent flow. As mentioned earlier, these include rapid fluid flow past sharp corners, angularities, or obstructions of some type and the mixing of different fluid streams. So, the improved nozzle design and analysis process consisted of modeling suspected turbulent generating nozzles and subsequent testing of these nozzles using the Huh Atomization Model[5]. This was done to determine if they possessed the proper turbulence exit conditions needed to produce an improvement over the baseline median secondary droplet size.

4.3.1 Nozzle Models

The add-on nozzles were modeled in a manner similar to the inhaler flow passages. The analysis tools and conditions were the same as the baseline inhaler internal flow passage. The grid generation method was consistent with all the models. The turbulent inlet conditions were set equal to the exit conditions of the inhaler internal flow passage model as seen in Figure 4.7. Water was chosen to simulate the flow of the drug as before. A zero normal-gradient boundary condition was used at the nozzle exit for all of the flow properties except pressure.

Inlet B.C.'s for add-on nozzle
Correspond to exit conditions of
inhaler baseline model
$Q=5.0e\text{-}06 \text{ m}^3/\text{s}$
$k=5.8 \text{ m}^2/\text{s}^2$
$\varepsilon=7.0e\text{+}04 \text{ m}^2/\text{s}^3$

Outlet B.C.'s for add-on nozzle
Outflow condition-assumes zero normal
gradient for all flow properties except
pressure (used when outlet conditions
aren't known and want to be solved for)

Figure 4.7. Schematic of add-on nozzle boundary conditions

In all of the add-on nozzle models, symmetry boundary conditions were used to speed up computational time and allow for an increased number of cells in the computational domain. The add-on nozzle models contain a consistent number of triangular cells (approximately 40,000). An example mesh from Multiple Inlet Nozzle 1 is shown in Figure 4.9. Again, the results of importance were the average k and ε values at the exit. These values were imported into the Huh Atomization Model[5] and a median secondary droplet size was predicted.

The nozzle types are classified into six different groups based on their geometric characteristics. The six groups are as follows:

Multiple Inlet Nozzles

These nozzles consist of two or four square or rectangular inlets that lead to a single outlet. Both the inlets and outlets could be straight or angled. The attempt was to get the flow to separate on inlet but converge to produce a single turbulent outlet. This nozzle would be produced out of two 500 μm chips that would be fused together after individual processing.

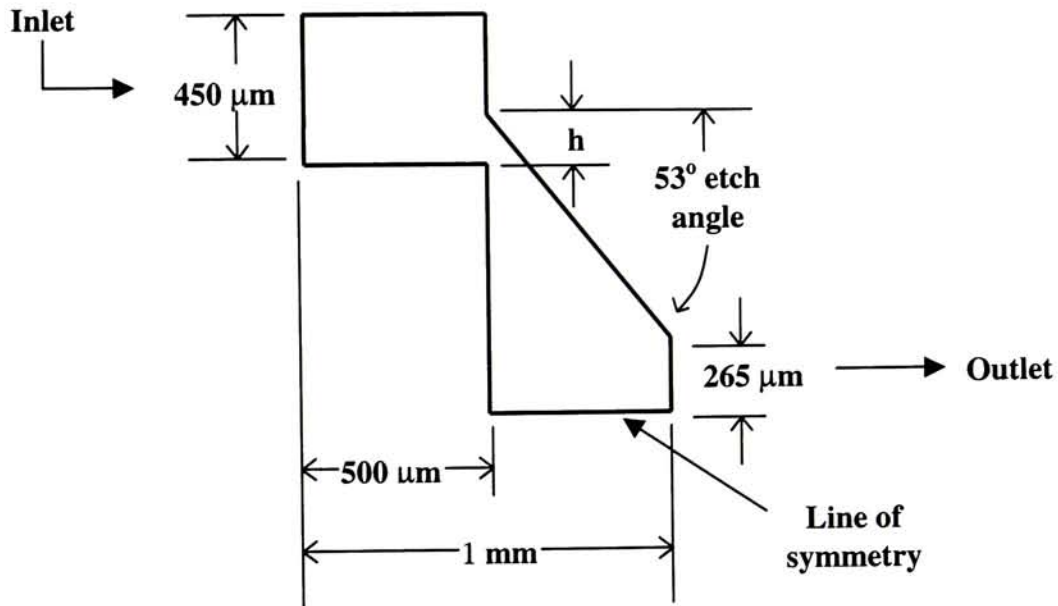The h-parameter is classified as the gap from the exit of the inlet chip to the inlet of the outlet chip.

Figure 4.8. Multiple inlet nozzle 1-four straight inlets, one angled outlet-h=150 μm
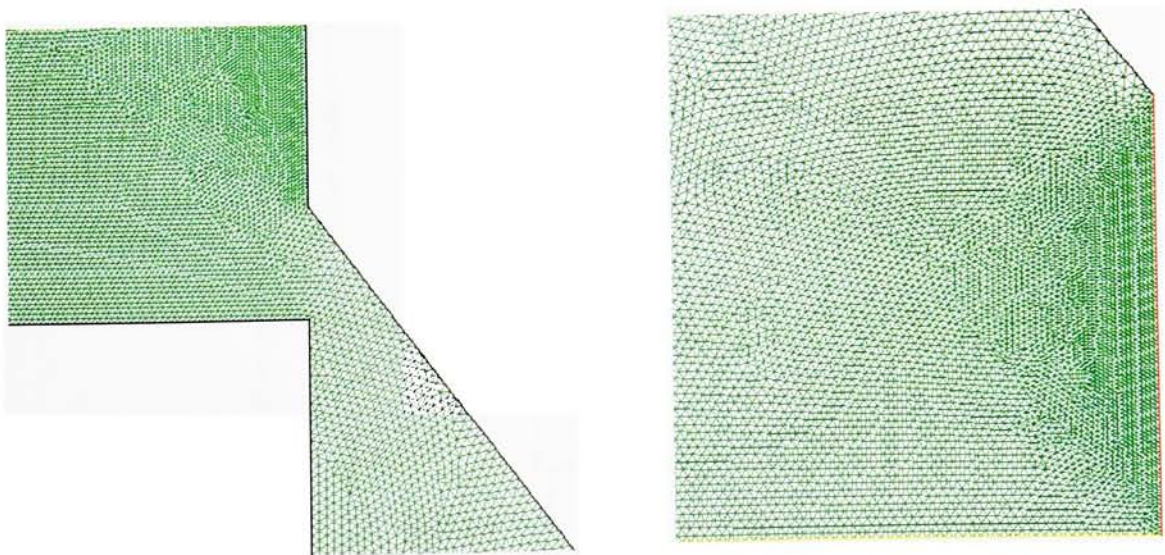

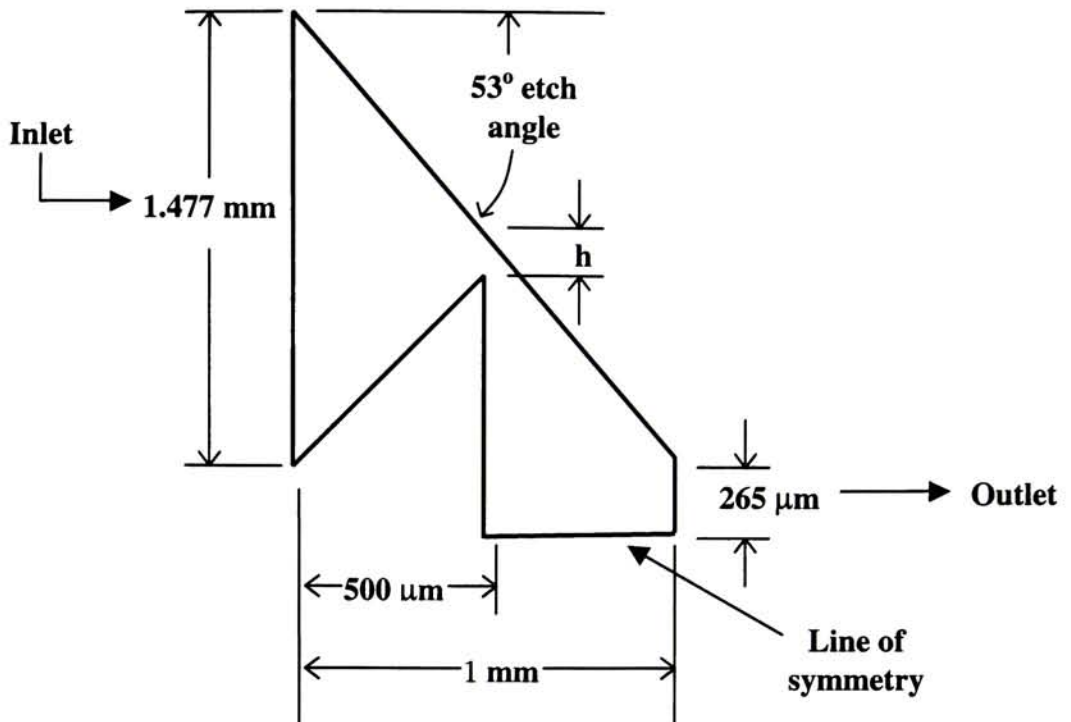**Figure 4.9. Multiple inlet nozzle 1 example mesh-inlet and h section (left), outlet section (right)**

Figure 4.10. Multiple inlet nozzle 2-version 1-two angled square inlets and one outlet-h=150 μm

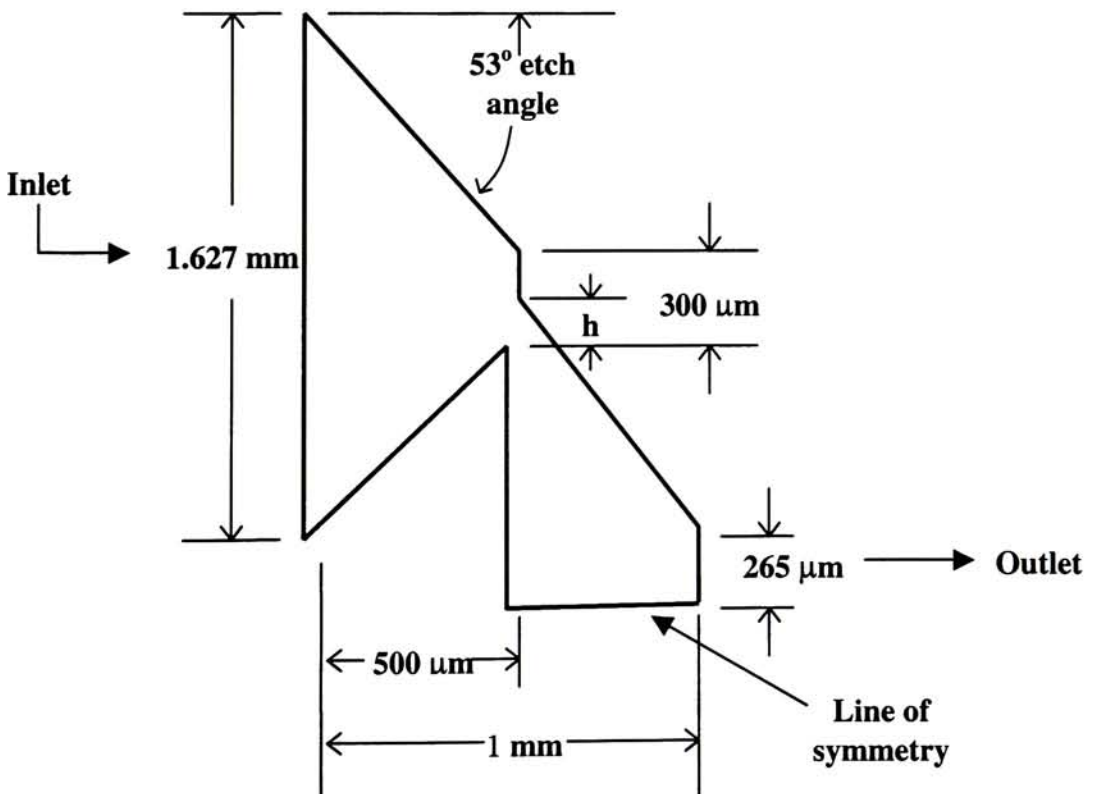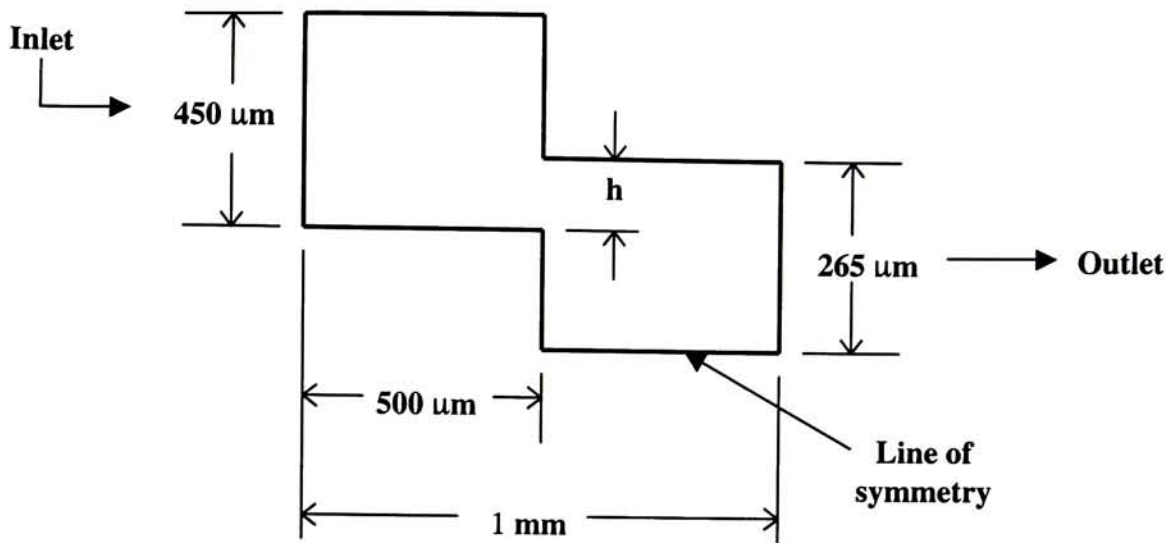**Figure 4.11. Multiple inlet nozzle 2-version 2-two offset angled inlets and one outlet- h=150 μm**

Figure 4.12. Multiple inlet nozzle 3-version 1-two straight square inlets and one outlet- h=150 μm

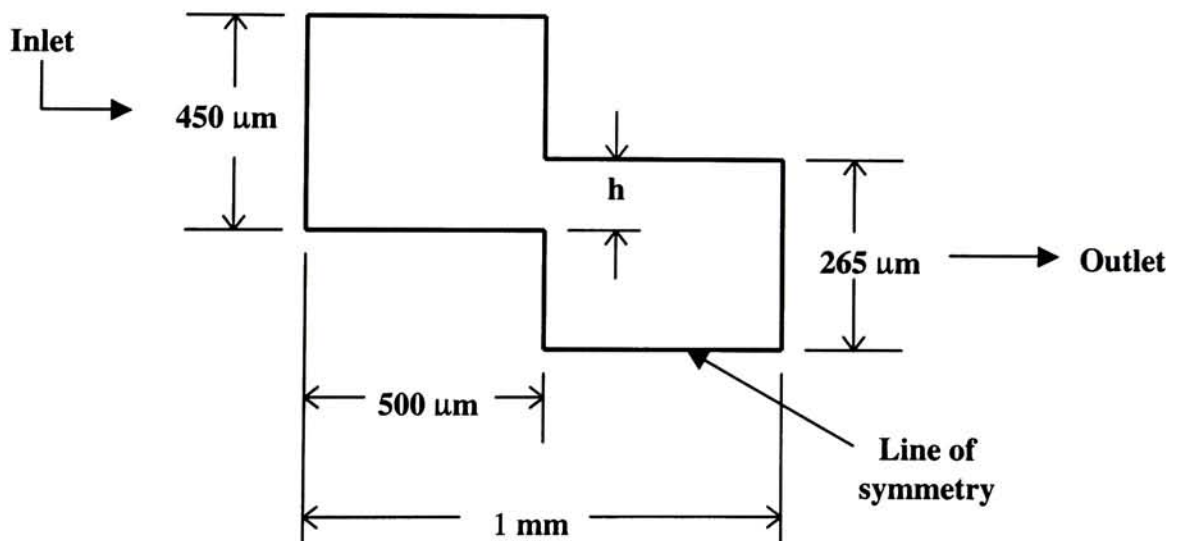**Figure 4.13. Multiple inlet nozzle 3-version 2-two straight square inlets and one outlet- h=100 μm**

W-Nozzle

This type of nozzle consists of one angled, rectangular inlet that forces the flow over a triangular-type obstruction into a single outlet. This nozzle would be produced out of two 500 μm chips that would be fused together after individual processing. The inlet chip geometry would be produced using an overlapping and angled etching strategy. This would hopefully lead to the desired geometry. Again, the attempt was to get the flow to separate over the obstruction but converge to produce a single turbulent outlet. The h-parameter is classified as the gap from the edge of the triangular obstruction to the side of the straight outlet.
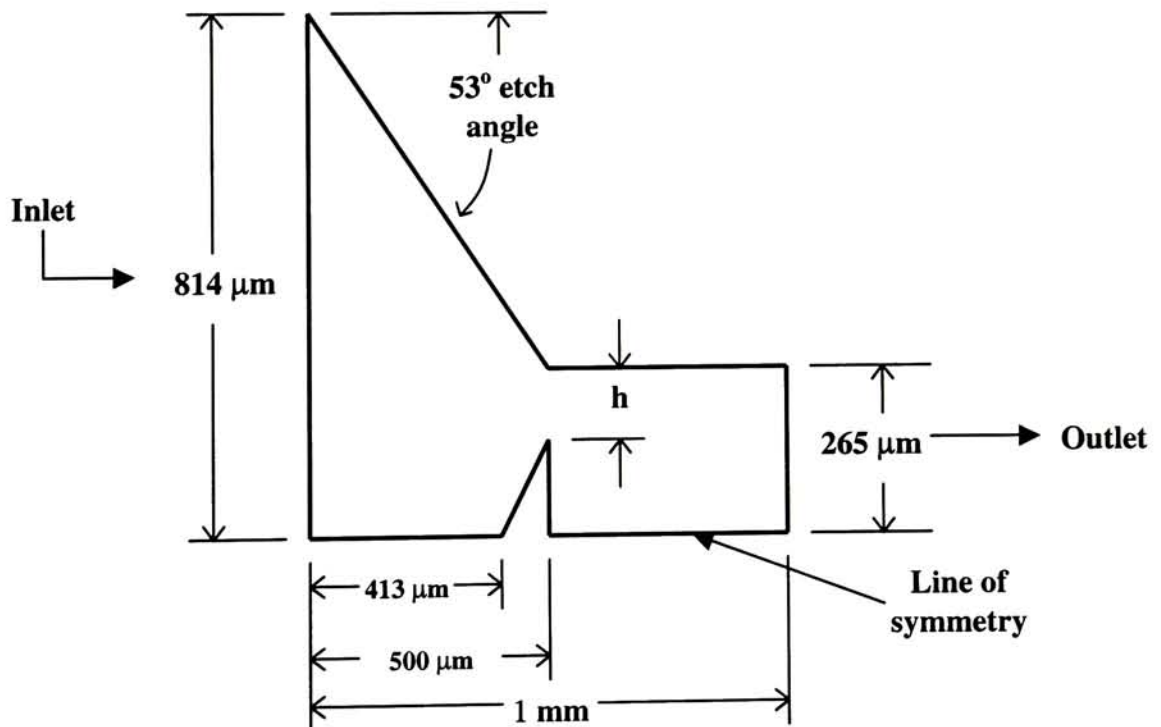
Figure 4.14. W-nozzle-version 1-one angled rectangular inlet and one outlet-h=150 μm
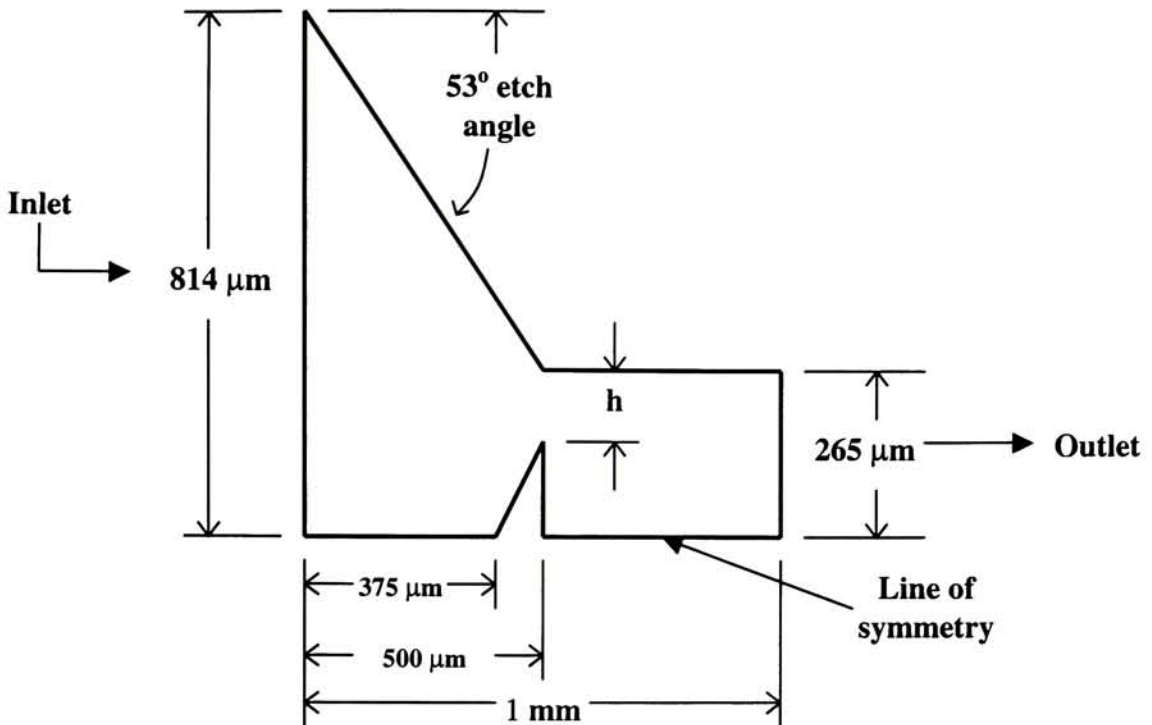
Figure 4.15. W-nozzle-version 2-one angled rectangular inlet and one outlet-h=100 μm

Mesh Nozzle

This nozzle is similar to the multiple inlets, however it would have many more inlets. The model shown in Figure 4.16 was designed with twelve inlets in mind. This design disturbs the flow and leads to turbulent conditions at the exit.
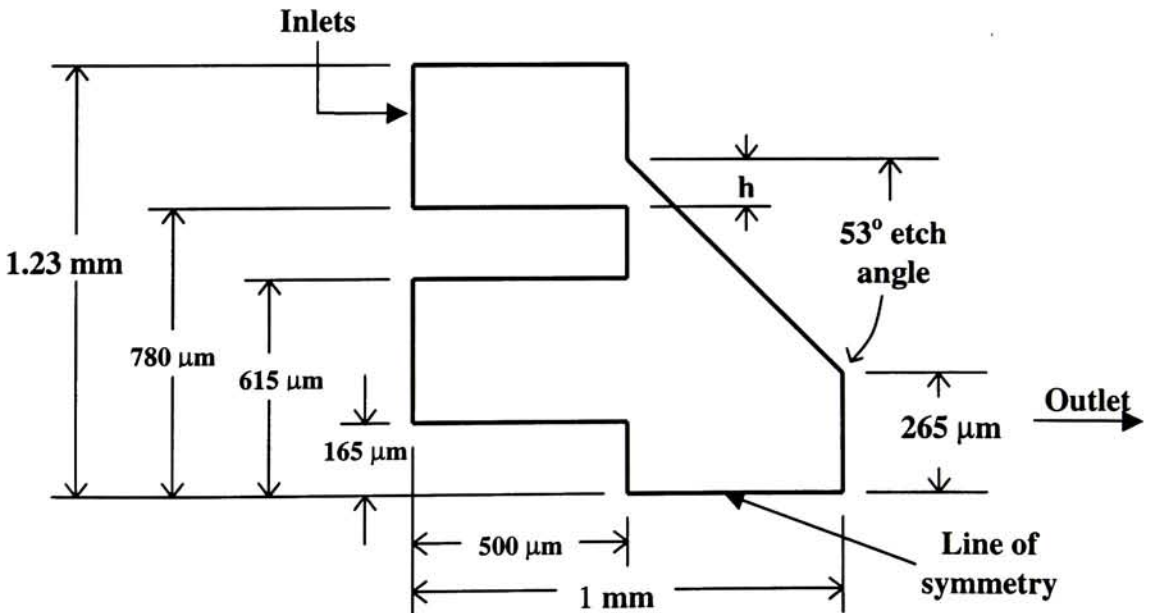
Figure 4.16. Mesh nozzle-twelve square inlets, one angled outlet-h= 150 μm

Simple Contraction Nozzle

This nozzle consists of a square inlet that converges to a throat and then flows into a divergent outlet. The throat distance is equal to 200 μm.

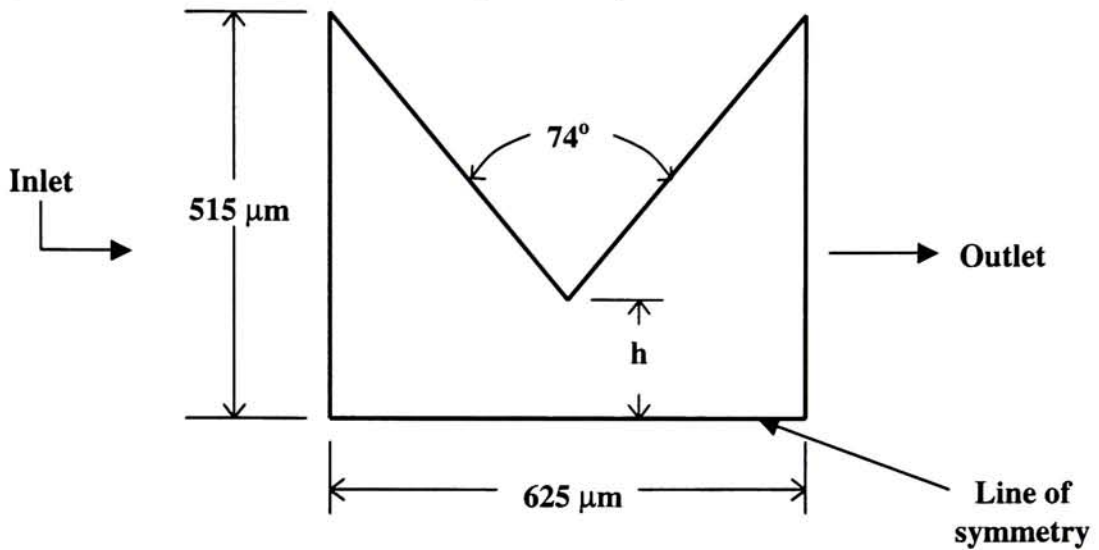**Figure 4.17. Simple contraction nozzle-square inlet and outlet-h=100 μm**

Stepped Nozzle

This nozzle consists of a series of step down sections that lead to square outlet. In this case, the step length was 500 μm.
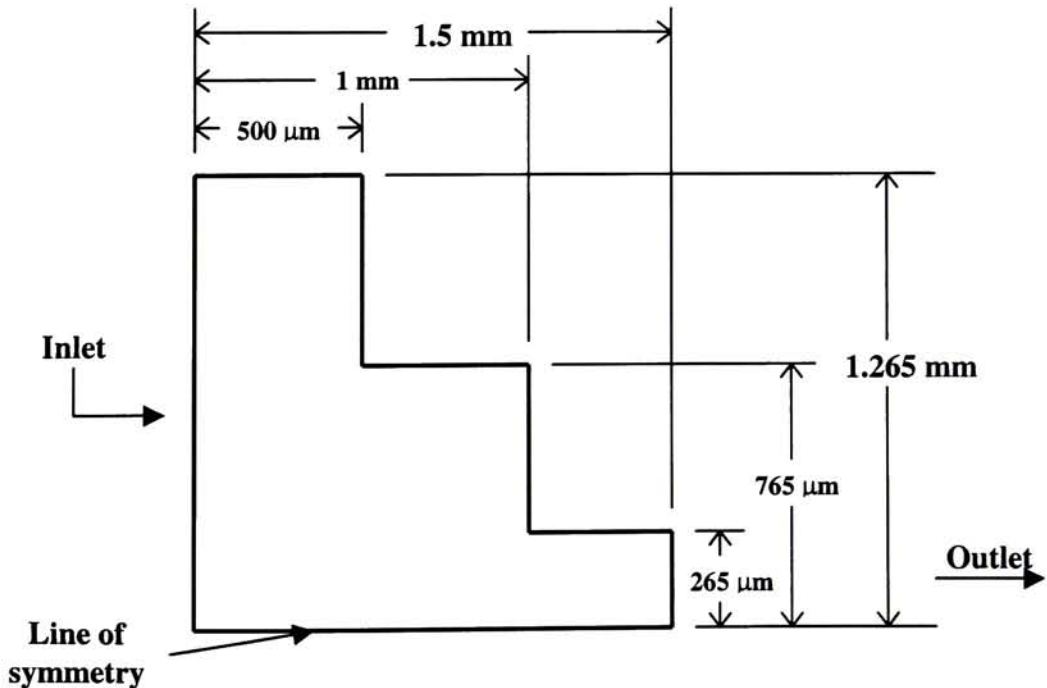
Figure 4.18. Stepped nozzle-square steps

Combination Multiple Inlet and Stepped Nozzle

This nozzle consists of a series of offset square sections that step down to the outlet. It would most likely contain two inlets.
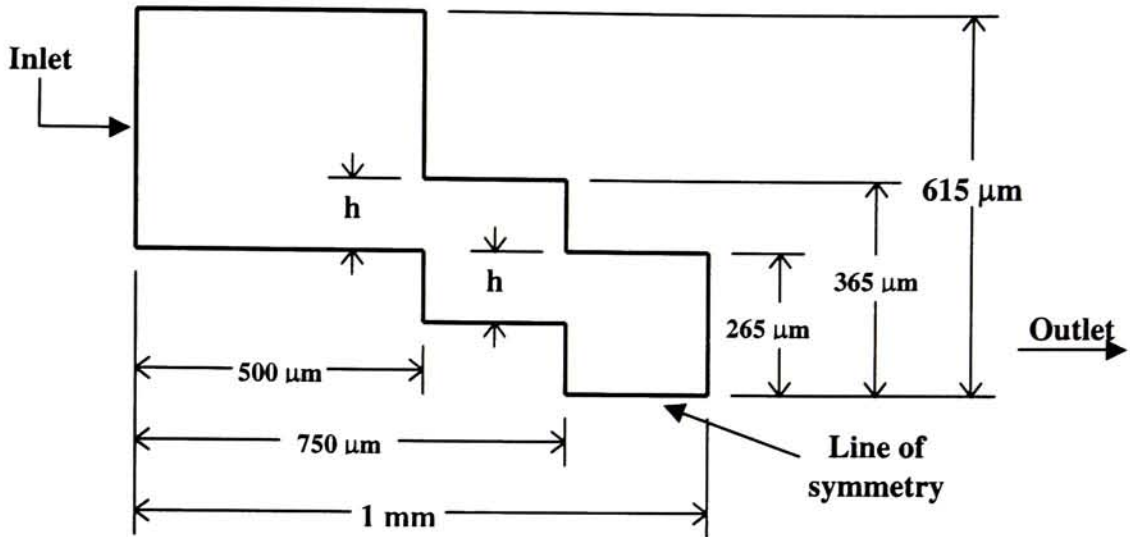
Figure 4.19. Combination multiple inlet and stepped nozzle-h=100 μm

4.3.2 Comparison of Add-on Nozzle Results

The results from the two-dimensional modeling of the initial add-on nozzles are shown in Table 4.1.

Nozzle	k_{avg}, m^2/s^2	ε_{avg}, m^2/s^3	$k_{avg}/\varepsilon_{avg}$ ratio	Projected median sec. drop size, μm
Multi-inlet 1	9.3	1.67e+06	5.57e-06	85
Multi-inlet 2,ver. 1	5.8	2.80e+05	2.07e-05	137
Multi-inlet 2,ver. 2	5.6	2.14e+05	2.62e-05	155
Multi-inlet 3,ver. 1	22.8	1.88e+06	1.21e-05	200
Multi-inlet 3,ver. 2	45.45	5.38e+06	8.45e-06	233
W-Nozzle,ver. 1	5.87	3.95e+05	1.49e-05	115
W-Nozzle,ver. 2	5.65	3.21e+05	1.76e-05	123
Mesh Nozzle	5.98	3.27e+05	1.83e-05	130
Simple Contract.	11.1	4.27e+05	2.59e-05	213
Stepped Nozzle	3.44	4.02e+04	8.56e-05	227

Multi-inlet & Step	140	3.18e+07	4.40e-06	285
Inhaler 2D Model	2.52	3.76e+04	6.70e-05	170

Table 4.1. Initial 2D nozzle modeling results

To ensure that the two-dimensional models captured the trend of the three-dimensional flow effects, three of the above nozzles were modeled in three dimensions and the results are shown in Table 4.2.

Nozzle	k_{avg}, m^2/s^2	ε_{avg}, m^2/s^3	$k_{avg}/\varepsilon_{avg}$ ratio	Exit Velocity, m/s	Projected median sec. drop size, μm
Multi-inlet 1	47.15	4.03e+06	1.17e-05	17.86	285
Inhaler	5.80	7.0e+04	8.29e-05	17.8	290
Multi-inlet 2,ver. 1	184	3.28e+07	5.61e-06	17	370

Table 4.2. Initial 3D nozzle modeling results

From the above results in can be seen that the lowest projected value for the median occurs in the Multi-inlet nozzle 1. This nozzle produces a low $k_{avg}/\varepsilon_{avg}$ ratio at a relatively low value of k_{avg} on exit from the nozzle. As seen earlier, this type of turbulence exit condition leads to the best results.

4.3.3 Optimization of Multi-inlet Nozzle 1

The Multi-inlet nozzle 1 gives the lowest secondary median droplet size among the add-on nozzles considered thus it was optimized. This involved changing two geometric parameters on the nozzle and quantifying the effects. These parameters were classified as the h and s dimensions. They were the only ones that could be changed since both the chip thickness and etch angles were fixed at 500 μm and 53°, respectively, due to the fabrication process (Appendix A). Also, the exit area was kept the same as the baseline inhaler model exit area to insure that the exit velocity was kept constant at around 17 m/s. The important dimensions are shown in Figure 4.20.
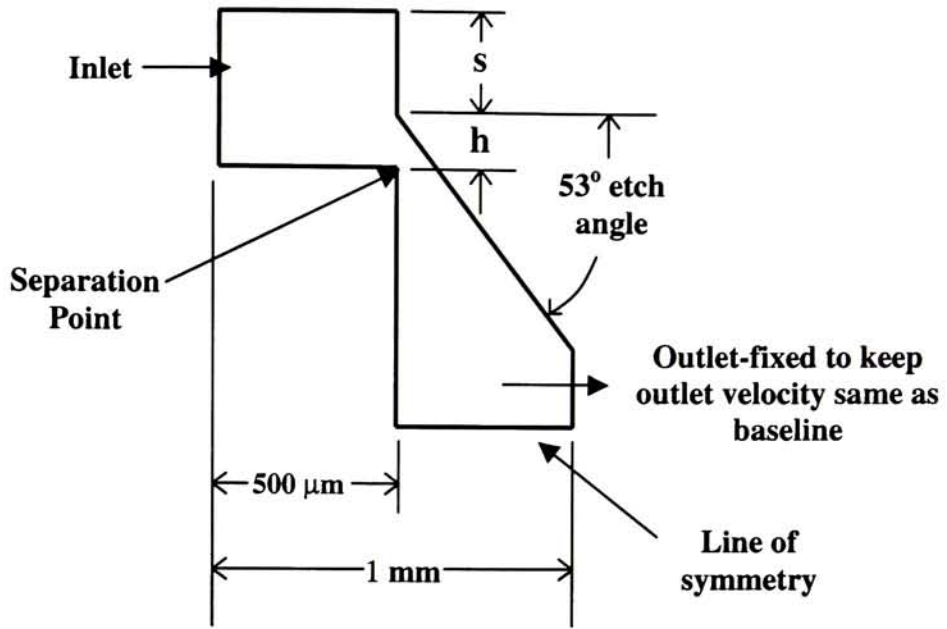
Figure 4.20. Multi-inlet nozzle 1 schematic

The h-parameter was varied from 150 μm down to 25 μm with the inlet velocity and outlet dimensions held constant. This optimization was modeled in both two and three-dimensions to ensure that the trend was consistent. The projected median was calculated for each h value considered. From Figure 4.21 we see that as the h value is increased beyond 100 μm the projected median tends to increase. This tendency continues as the h value is decreased below 100 μm. Thus, the optimum value for h occurs around 100 μm. This result is consistent in both the two-dimensional and three-dimensional analysis.
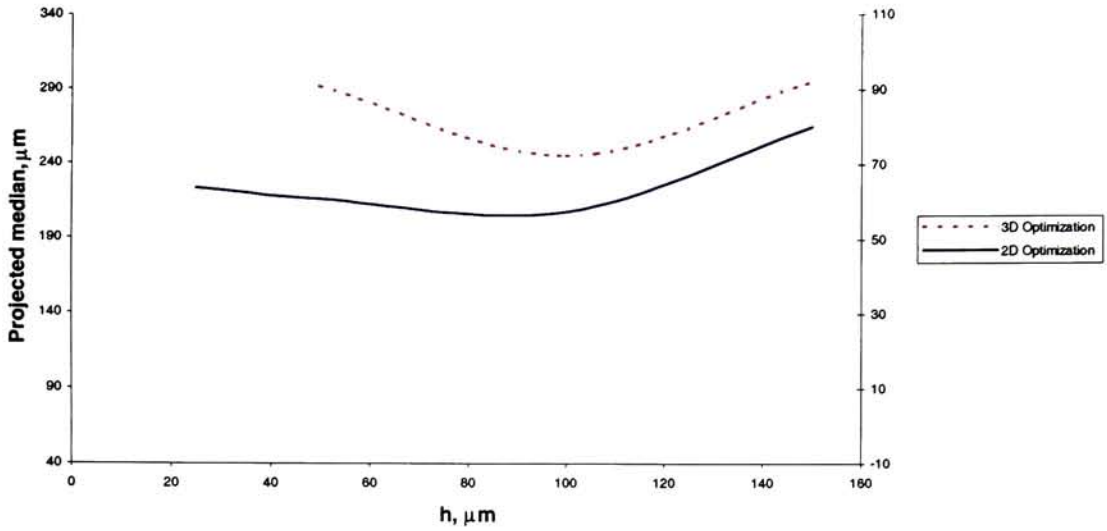
Figure 4.21. Optimization results for geometric parameter, h

The s-dimension was varied from 100 µm to 450 µm at three different constant values of h, namely 150 µm, 100 µm, and 50 µm. These results are shown in Figure 4.22. The three curves exhibit the same behavior. There is an s value associated with a minimum median droplet size for each h curve. As s is increased above and below this value, the projected median increases. It is seen that the optimum value for s occurs at approximately 350 µm at an h value of 100 µm. These results are consistent with the previous h optimization.
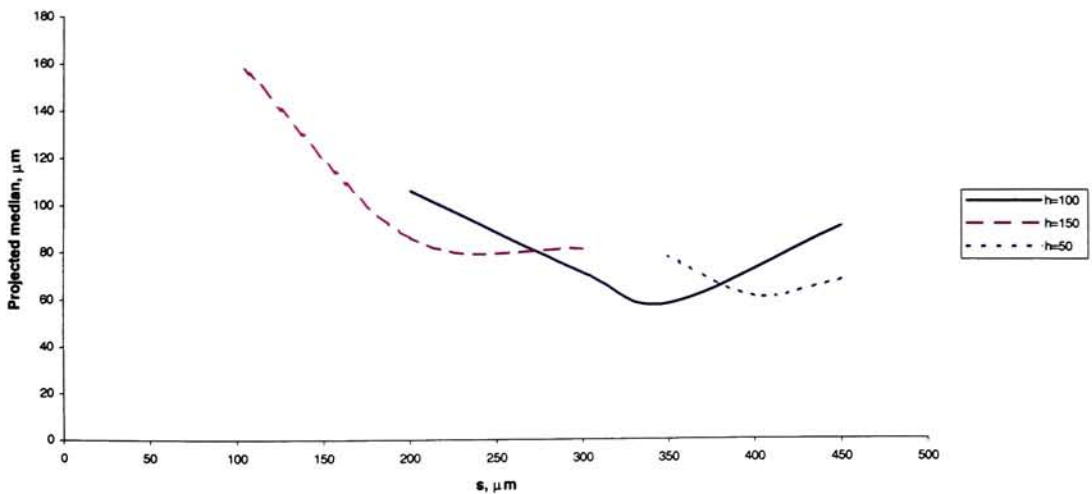
Figure 4.22. Optimization results for geometric parameter, s

The Multiple Inlet Nozzle 1 contains four straight inlets on one chip leading to a single angled outlet on the second chip. It seems that this combination dissipates k rapidly and doesn't allow for the transport of large values of k to the exit of the nozzle (i.e. low $k_{avg}/\varepsilon_{avg}$ ratio at a low value of k_{avg}). The presence of the angled wall immediately after the inlet section acts to rapidly change the fluctuating components of velocity and thus k (leads to high ε). The turbulent eddies that are set up following the separation point are broken up into eddies of much smaller size due to the confining effect of the angled outlet (i.e. high ε_{avg} and lower k_{avg} on exit). An h value of 100 µm and an s value of 350 µm produce the optimum results. At larger h values, the turbulent eddies don't seem to impact the confining wall enough to break up into the proper size (ε is not high enough). At smaller h values, the localized velocity is too high to allow for break up against the wall before the turbulent eddies are transported downstream to the exit (k is too high).

4.3.4 3D Model of Multiple Inlet Nozzle 1

The optimum values for the h and s parameters had been determined to be 100 µm and 350 µm, respectively, from Section 4.3.3. A three-dimensional version of the optimum Multiple Inlet Nozzle 1 was modeled and an improved median secondary droplet size was predicted. The modeling procedure was the same as the previous nozzles. The model consists of four square inlets with an inlet area of 2.025e-07 m^2 each. A schematic of the 3D model is shown in Figure 4.23.
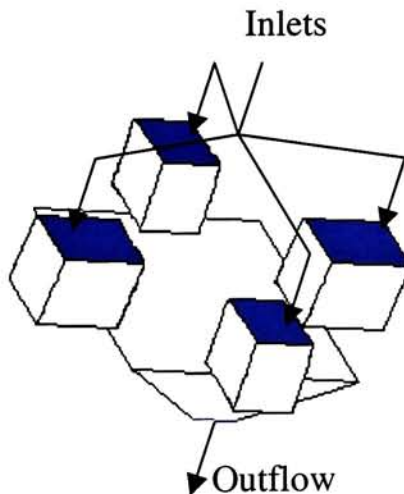

Inlets

Outflow

Figure 4.23. 3D schematic of multiple inlet nozzle 1

With a flow rate of 5.0e-06 m^3/s and the inlet area mentioned above, this leads to an inlet velocity of 6.17 m/s. The turbulent inlet conditions were set equal to the exit conditions of the inhaler internal flow passage model (k_{avg}=5.8 m^2/s^2, ε_{avg}=7.0e+04 m^2/s^3). The exit area was kept equal to that of the baseline inhaler exit area of 2.83e-07 m^2. This was to keep the outflow velocity approximately the same. This nozzle is symmetric about two planes of symmetry so, only one fourth of the nozzle was actually modeled. The results were checked for grid independence and the final mesh contains approximately 230,000 triangular volume elements.

The results of importance from this analysis include the turbulent kinetic energy (k) and the turbulent kinetic energy dissipation rate (ε). Flow contours of the computational results are shown in Figures 4.24 and 4.25.

Figure 4.24 illustrates the contours of turbulent kinetic energy. The main point of interest is at the outflow location.
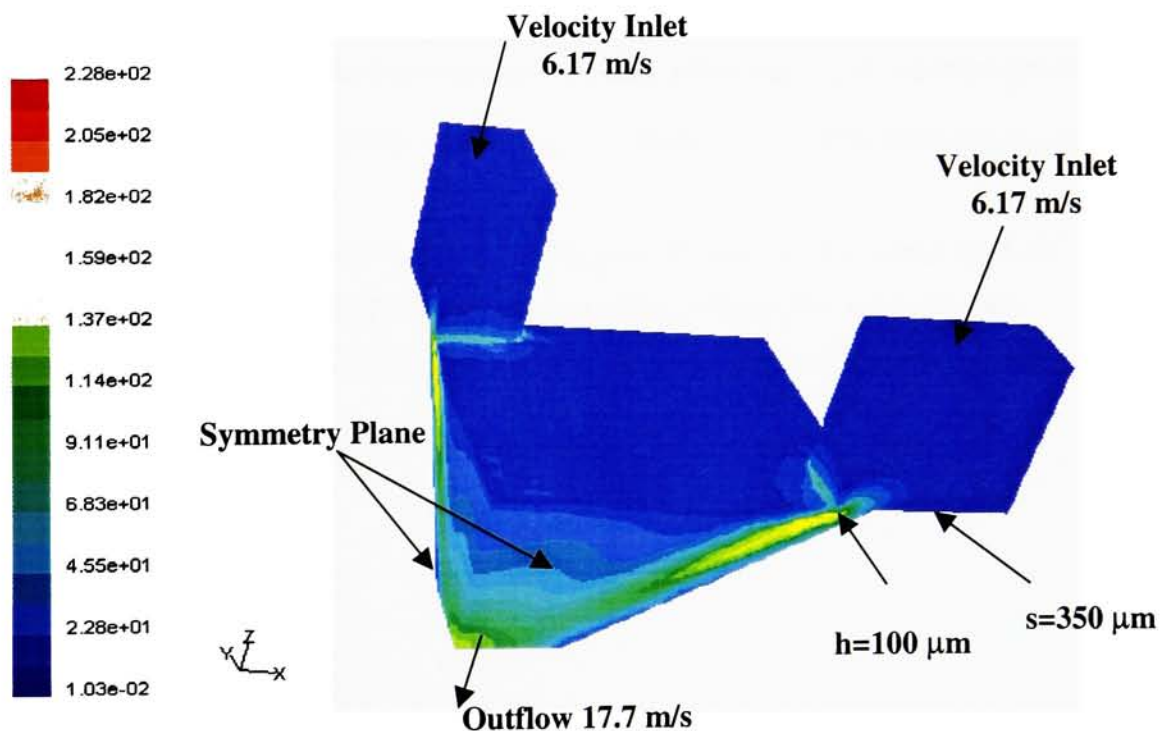
Figure 4.24. Multiple inlet nozzle 1-turbulent kinetic energy, k_{avg} on exit =60.8 m^2/s^2

From a vertex average on outflow of the nozzle, k_{avg} =60.8 m^2/s^2.
Figure 4.25 shows the flow contours of ε for the Multiple Inlet Nozzle 1. Again, the area of concern is at the nozzle exit.
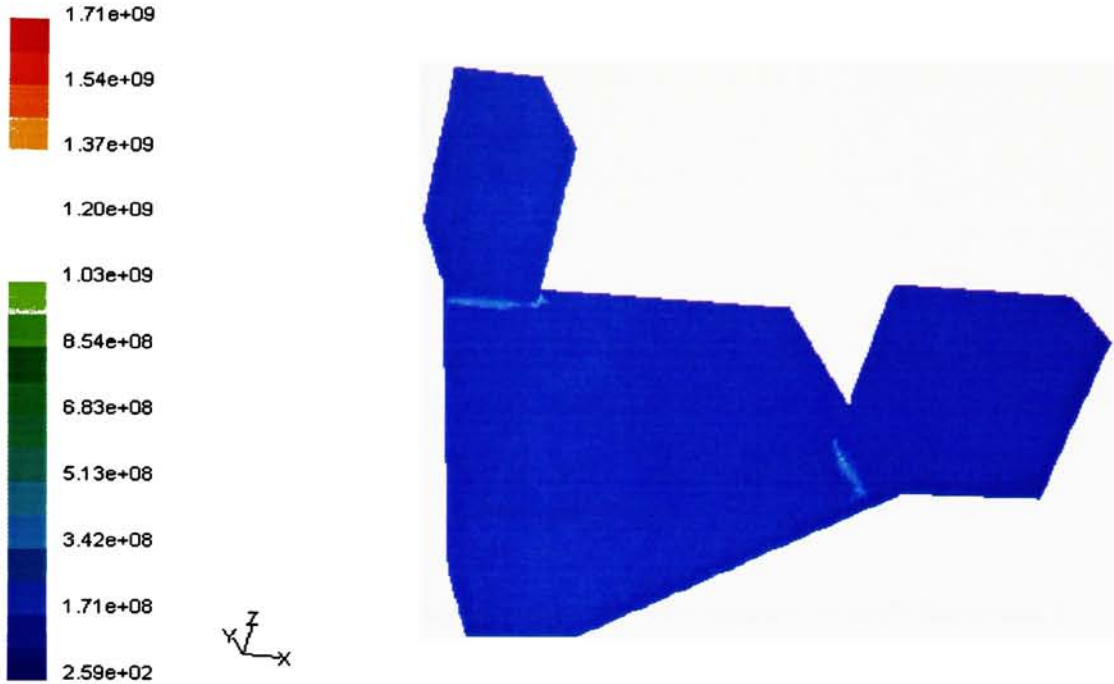
Figure 4.25. Multiple inlet nozzle 1-turbulent kinetic energy dissipation, ε_{avg} on exit=8.13e+06 m^2/s^3

From a vertex average on exit of the nozzle, $\varepsilon_{avg} = 8.13e+06$ m^2/s^3. This leads to a $k_{avg}/\varepsilon_{avg}$ ratio of 7.48e-06.

The turbulence exit conditions (k_{avg} and ε_{avg}) of the nozzle were used to find the probability density function (PDF) and median secondary droplet size from the Huh Atomization Model[5]. Figure 4.26 illustrates the PDF for $k_{avg} = 60.8$ m^2/s^2 and $\varepsilon_{avg} = 8.13e+06$ m^2/s^3.
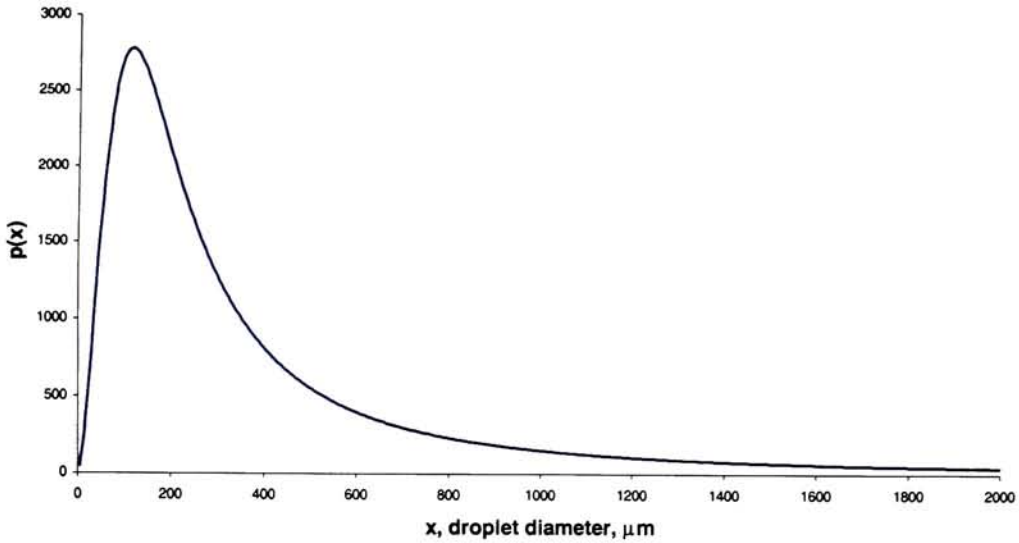
Figure 4.26. Secondary droplet size distribution for optimized multiple inlet nozzle 1

The cumulative secondary drop size distribution, F(x) can be calculated from the PDF and this is shown in Figure 4.27.
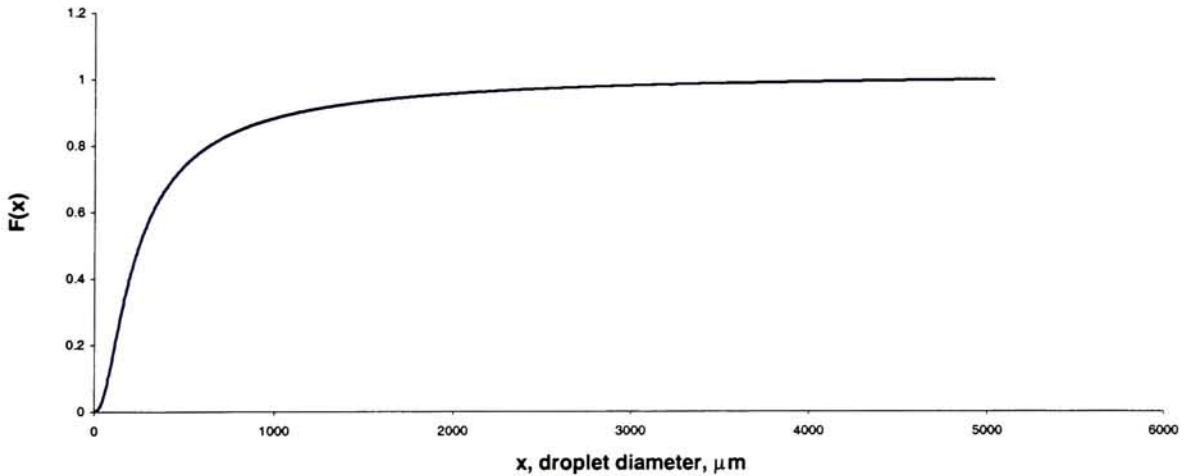
Figure 4.27. Cumulative secondary drop size distribution for optimized multiple inlet nozzle 1

The area under the PDF is set equal to 1.0 through the use of the normalization constant (Equation 3.2) described in Section 3.4.1. It follows then that the median is the droplet diameter at which the area under the PDF is equal to 0.5. This is the same point at which the

cumulative size distribution $(F(x))$ will be equal to 0.5. The median secondary droplet size resulting from the optimized Multiple Inlet Nozzle 1 was 245 μm.

4.4 Summary of Results

The purpose of this study was to design and analyze turbulence generating nozzles for the improvement of existing pressurized metered dose inhaler therapy. The existence of turbulence within the inhaler nozzle is one mechanism that leads to the production of the aerosol in this device. The current inhaler internal flow passage was analyzed on a turbulence basis and a baseline median secondary droplet size of 290 μm was predicted. The analysis of the Huh Atomization Model[5] led to the conclusion that changing the turbulence exit conditions in the inhaler through the addition of a nozzle could lead to a reduced median secondary droplet size. The existence of a low $k_{avg}/\varepsilon_{avg}$ ratio at a relatively low value of k_{avg} on exit from the nozzle produces the desired results. This means that the majority of the turbulent energy of the flow is contained in eddies of a small size. Eleven different nozzles were tested in an effort to achieve these results. It was found that a nozzle of the type of Multiple Inlet Nozzle 1 had the most potential and was thus optimized to generate the best results. The addition of the Multiple Inlet Nozzle 1 leads to a 15.5% reduction in the median secondary droplet size based on the development of the proper turbulence exit conditions alone. It is important to note again that this analysis was based solely on generation of turbulence within the nozzles. The relative improvement achieved with the new add-on nozzles compared with that of the baseline inhaler model was the main objective. The actual droplet size is expected to be smaller due to the influence of the other atomization mechanisms (flashing of propellant and formulation properties) associated with spray formation in the pMDI.

Chapter 5-Conclusions

Pharmaceutical inhalation aerosol technology has become an important therapy for the treatment of both respiratory and non-respiratory illness. Targeting therapeutic aerosols to the small airways of the lung can effectively treat many of these diseases. Delivery of the therapeutic agent directly to the site of action, for cases involving respiratory diseases, ensures an adequate therapeutic level of the drug is reached, without leading to side effects due to high systemic concentrations. For non-respiratory diseases, the periphery of the lung offers enormous surface area (approximately $100m^2$) for rapid absorption into circulation.[17] In either case, the appropriate spray characteristics ($0.5 \mu m < MMAD < 5 \mu m$[1,2,3,4] and as low velocity as possible) are vital to targeting the lung periphery.

There are three major categories of medical inhalation devices currently in use. All of them have their advantages and drawbacks. They consist of the Pressurized Metered-Dose Inhaler (pMDI), the Dry Powder Inhaler (DPI), and the Nebulizer. Of the three inhalation devices described above, the pMDI is the most commonly prescribed method of aerosol delivery.[14,28] The pMDI is inexpensive, portable, and at least as effective as other systems of aerosol generation for drug delivery, if properly used.[14,29] Thus, with further improvements, it could become the most optimal and desirable means of drug delivery to the lungs.

Within pressurized metered dose inhalers (pMDI), many factors lead to the break-up or atomization of the formulation. These include the nozzle geometry, volatilization of the propellant (cavitation), and turbulence in the nozzle. No single atomization model has been developed to account for all of these factors. Models have been developed to account for the flashing of the propellant as the primary atomization mechanism.[45,46] This study was concerned with the positive effects of turbulence generation so, the Huh Atomization Model[5] was used to predict the droplet size distribution resulting from certain nozzle exit conditions. This model considers both turbulence and wave growth as important processes in atomization.

The purpose of this study was to design and analyze turbulence generating add-on nozzles for the improvement of existing pressurized metered dose inhaler therapy (namely,

reducing the median droplet size at a similar exit velocity). The development of the proper turbulence characteristics on exit from the nozzles was a key factor in promoting greater atomization and reducing the median droplet size. Geometries were created to separate the flow and create regions of vorticity and rotation in the nozzles. These regions hold energy-containing turbulent eddies of various sizes that are vital to the atomization process and resulting spray distribution. Analysis of the Huh Atomization Model[5] showed that producing a low $k_{avg}/\varepsilon_{avg}$ ratio at a relatively low value of k_{avg} could reduce the median droplet size. In practical terms, increasing ε_{avg} for a constant value of k_{avg} produces a shift in the energy containing eddies from larger to smaller sizes. Smaller eddies are more efficient in dissipating energy than larger ones[50], so the turbulent kinetic energy is concentrated in eddies of smaller sizes, which ultimately produces a reduced median secondary droplet size.

Eleven different nozzles were tested in an effort to achieve these results. The Multiple Inlet Nozzle 1 had the most potential and was thus optimized to generate the best outcome (i.e. lowest median secondary drop size). This nozzle contains four straight inlets leading to a single angled outlet. It seems that this combination dissipates k rapidly and doesn't allow for the transport of large values of k to the exit of the nozzle (i.e. low $k_{avg}/\varepsilon_{avg}$ ratio at a low value of k_{avg}). The presence of the angled wall immediately after the inlet section acts to rapidly change the fluctuating components of velocity and thus k (leads to high ε). The turbulent eddies that are set up following the separation point are broken up into eddies of much smaller size due to the confining effect of the angled outlet (i.e. high ε_{avg} and lower k_{avg} on exit). The optimization of Multiple Inlet Nozzle 1 was based on two geometric parameters, namely h and s. An h value of 100 μm and an s value of 350 μm produce the most favorable results. At larger h values, the turbulent eddies don't seem to impact the confining wall enough to break up into the proper size (ε is not high enough). At smaller h values, the localized velocity is too high to allow for break up against the wall before the turbulent eddies are transported downstream to the exit (k is too high). Development of these proper turbulence characteristics with the addition of Multiple Inlet Nozzle 1 led to a 15.5% reduction of the representative secondary median droplet size resulting from the pMDI based on turbulence effects alone.

This thesis was the preliminary work in the investigation into the positive impacts that the addition of a turbulence-generating nozzle could have on the resulting pMDI spray.

Follow-up work will be needed to complete the investigation and some suggestions for that work are as follows:

First, the fabrication of the turbulence generating nozzles in this study followed by subsequent experimentation is a logical next step. This will also involve the design of the interface between the add-on nozzle and the existing inhaler. Second, modeling of the other factors involved in the aerosol production from the pMDI is a noteworthy task. This could include the primary atomization mechanism of volatilization of the propellant, which is related to evaporation or cavitation effects. Third, many drug formulations are suspensions of drug particles and not solutions. Modeling of this fact might involve setting up a two-phase Lagrangian flow of drug particles within the inhaler. And lastly, the design, development, and testing of other turbulence generating nozzles not mentioned in this investigation could prove to be of importance.

References

1. Suarez S, Hickey AJ. Drug Properties Affecting Aerosol Behavior. Respir Care 2000;45(6):652-666.

2. Byron PR, Patton JS. Drug Delivery Via the Respiratory Tract. J Aerosol Med 1994;7(1):49-75.

3. Brain JD, Valberg PA. Deposition of Aerosols in the Respiratory Tract (review). Am Rev Respir Dis 1979;120(6):1325-1373.

4. Zainudin BM. Therapeutic Aerosol: Principles and Practices. Med J Malaysia 1993;48(3):259-268.

5. Huh KY, Lee EJ, Koo JY. Development of a Diesel Spray Atomization Model Considering Nozzle Exit Turbulence Conditions. Atomization and Sprays 1998;8(4):453-469.

6. Newhouse MT. Tennis Anyone? The Lungs as a New Court for Systemic Therapy. CMAJ November 1999;161(10):1287-1288.

7. Sharma S, White D, Imondi AR, Placke ME, Vail DM, Kris MG. Development of Inhalational Agents for Oncologic Use. J Clin Oncol 2001;19(6):1839-1847.

8. Toso C, Williams DM, Noone PG. Inhaled Antibiotics in Cystic Fibrosis: A Review. Ann Pharmacother 1996;30(7-8):840-50.

9. Thompson PJ. Drug Delivery to the Small Airways. Am J Respir Crit Care Med 1998;157(5):S199-S202.

10. Howarth PH. Why Particle Size Should Affect Clinical Response to Inhaled Therapy. J Aerosol Med 2001;14(1):27(8 pages).

11. Gonda I, Byron P. Aerosols for Delivery of Therapeutic and Diagnostic Agents to the Respiratory Tract. Critical Reviews in Therapeutic Drug Carrier Systems 1990;6(4):273-300.

12. Mandal T. Module 8: Miscellaneous Preparations. Available From: <http://xavier.xula.edu/tmandal/pharmaceutics/aerosols.html> [Accessed August 2001].

13. Sanjar S, Matthews J. Treating Systemic Diseases via the Lung. J Aerosol Med 2001;14(1):51(8 pages).

14. Fink JB. Metered-Dose Inhalers, Dry Powder Inhalers, and Transitions. Respir Care 2000;45(6):623-635.

15. Wiener MV. How to Formulate Aerosols to Obtain the Desired Spray Pattern. Soc Cos Chem 1958;9:289-297.

16. Dhand R, Malik SK, Balakrishnan M, Verma SR. High Speed Photographic Analysis of Aerosols Produced by Metered-Dose Inhalers. J Pharm Pharmacol 1988;40(6):429-430.

17. Ariyananda PL, Agnew JE, Clarke SW. Aerosol Delivery Systems for Bronchial Asthma. Postgrad Med J 1996;72(845):151-156.

18. Newman SP. Aerosol Generators and Delivery Systems. Respir Care 1991;36(9):939-951.

19. Dolovich M, Ruffin RE, Roberts R, Newhouse MT. Optimal Delivery of Aerosols from Metered Dose Inhalers. Chest 1981;80(6 Suppl):911-915.

20. Berg E. In Vitro Properties of Pressurized Metered Dose Inhalers with and without Spacer Devices. J Aerosol Med 1995;8(3):S3-S11.

21. Dolovich M, Rheim R, Rashid F, Coates G, Hill M, Bowen B. Measurement of the Particle Size and Dosing Characteristics of a Radiolabelled Albuterol-Sulphate Lactose Blend used in the SPIROS Dry Powder Inhaler. In: Dalby RN, Byron P, Farr SY, editors. Respiratory Drug Delivery V. Buffalo Grove: Interpharm Press;1996:332-335.

22. Engel T, Heinig JH, Madsen F, Nikander K. Peak Inspiratory Flow and Inspiratory Vital Capacity of Patients with Asthma Measured with and without a New Dry-Powder Inhaler Device (Turbuhaler). Eur Respir J 1990;3(9):1037-1041.

23. Brian JD, Valberg PA. Deposition of Aerosols in the Respiratory Tract (Review). Am Rev Respir Dis 1979;120(6):1325-1373.

24. Zainudin BM. Therapeutic Aerosols: Principles and Practices. Med J Malaysia 1993;48(3):259-268.

25. Wolff RK, Niven RW. Generation of Aerosolized Drugs. J Aerosol Med 1994;7(1):89-103.

26. Hess DR. Nebulizers: Principles and Performance. Respir Care 2000;45(6):609-622.

27. Greenspan BJ. Ultrasonic and Electrohydrodynamic Methods for Aerosol Generation. In: Hickey AJ, editor. Inhalation Aerosols: Physical and Biological Basis for Therapy. New York: Marcel Decker; 1996:313-335.

28. Fink JB, Dhand R. Aerosol Therapy. In: Fink JB, Hunt G, editors. Clinical Practice in Respiratory Care. Philadelphia: Lippincott Raven; 1998.

29. AARC Clinical Practice Guideline: Selection of and Aerosol Delivery Device. Respir Care 1992;37(8):891-897.

30. Atkins PJ. Aerodynamic Particle-Size Testing-Impinger Methods. Pharm Tech 1992;16:26-32.

31. Milosovich SM. Particle-Size Determination via Cascade Impaction. Pharm Tech 1992;16:82-86.

32. Mitchell JP, Nagel MW, Archer AD. Performance Testing of a New Low Flow Marple-Miller Cascade Impactor. Respiratory Drug Delivery VI 1998;381-383.

33. Mitchell JP. The Next Generation Impactor (NGI): Results from the Evaluation of Prototype Instruments with Pressurized Metered Dose Inhaler (pMDI)-Based Formulations. Drug Delivery to the Lungs XI. J Aerosol Med 2001;14(1):133.

34. Evans R. Determination of Drug Particle Size and Morphology Using Optical Microscopy. Pharm Tech 1993;17:146-152.

35. Dhand R, Malik SK, Balakrishnan M, Verma SR. High Speed Photographic Analysis of Aerosols Produced by Metered Dose Inhalers. J Pharm Pharmacol 1988;40:429-430.

36. Gorman WG, Carroll FA. Aerosol Particle Size Determination Using Laser Holography. Pharm Tech 1993;17:34-37.

37. Niven RW. Aerodynamic Particle Size Testing Using a Time-of-Flight Aerosol Beam Spectrometer. Pharm Tech 1993;17:72-78.

38. Mitchell JP, Nagel MW, Archer AD. Size Analysis of a Pressurized Metered Dose Inhaler (pMDI)-Delivered Suspension Formulation by the API Aerosizer® Time-of-Flight Aerodynamic Particle Size Analyzer. J Aerosol Med 1999;12(4):255-264.

39. Myrdal PB, Gupta A, Stein SW, Gabrio BJ, Beck TJ. Evaluation of a New Aerodynamic Particle Sizer for MDI Size Distribution Measurements. Respiratory Drug Delivery VIII Volume II 2002;663-666.

40. Ranucci J. Dynamic Plume-Particle Size Analysis Using Laser Diffraction. Pharm Tech 1992;16:109-114.

41. Dunbar CA, Watkins AP, Miller JF. An Experimental Investigation of the Spray Issued from a pMDI Using Laser Diagnostic Techniques. J Aerosol Med 1997;10(4):351-368.

42. de Boer AH, Gjaltema D, Witt W, Frijlink HW. The Use of a Laser Diffraction Technique for the Characterization of the Aerosol Cloud from Inhalation Devices. Respiratory Drug Delivery VII Volume II 2000;585-588.

43. Wachtel H, Ziegler J. Improved Assessment of Inhaler Device Performance Using Laser Diffraction. Respiratory Drug Delivery VIII Volume II 2002;379-382.

44. Clark AR. MDIs: Physics of Aerosol Formation. J Aerosol Med 1996;9 Suppl:S19-S26.

45. Clark AR. Metered Atomization for Respiratory Drug Delivery. PhD Thesis 1991. Loughborough University of Technology, Loughborough, UK.

46. Dunbar CA, Watkins AP, Miller JF. Theoretical Investigation of the Spray from a Pressurized Metered Dose Inhaler. Atomization and Sprays 1997;7:417-436.

47. Mathieu J, Scott J. An Introduction to Turbulent Flow. New York: Cambridge U. Press, 2000.

48. Richardson WP. The Influence of Upstream Flow Conditions on the Atomization Performance of a Low Pressure Port Fuel Injector. Masters Thesis 1991. Michigan Technical University.

49. Chen CJ, Jaw SY. Fundamentals of Turbulence Modeling. Washington, DC: Taylor & Francis, 1998.

50. Garde RJ. Turbulent Flow. John Wiley & Sons, 1994.

51. Star-CD Users Manuals. Methodology Guide V3-10.

52. Lefebvre AH. Atomization and Sprays. Bristol, PA: Taylor & Francis, 1989.

53. Ohnesorge W. Formation of Drops by Nozzles and the Breakup of Liquid Jets. Z Angew Math Mech 1936;16:355-358.

54. Reitz RD. Atomization and Other Breakup Regimes of a Liquid Jet. PhD Thesis 1978. Princeton University, Princeton, NJ.

55. Groover MP. <u>Fundamentals of Modern Manufacturing: Materials, Processes, and Systems.</u> Upper Saddle River, NJ: Prentice-Hall, 1996.

Appendix A-Manufacturing Process

It was clear to me that the new nozzles would contain holes and passageways of a small nature. So, it became apparent that etching in a silicon chip in a manner similar to Integrated Circuit production on a microchip would be a feasible manufacturing process. This process imposed certain restrictions on the nozzle designs (namely max thickness of 500µm for one chip, and an etch angle of either $53.4°$ or $90°$). It was vital to keep this manufacturing process in mind in the thought process for the design of the add-on nozzles. The basic steps to this process are as follows:

First, a silicon wafer is cut from a large silicon ingot. These wafers are typically 500 µm thick. Second, the surface of the silicon wafer is oxidized to produce of barrier layer of SiO_2. Third, the surface is prepared and photoresist is applied. A photoresist is an organic polymer that is sensitive to light radiation in a certain wavelength range.[55] It comes in both positive and negative types. The type of photoresist refers to what happens to the material after it is exposed. The positive type becomes more soluble in a developing solution and the negative type is less soluble. Fourth, after a soft bake, a pattern mask is aligned to the wafer and the resist is exposed to a certain type of light. This process basically transfers an image onto the surface of the photoresist material. Fifth, the resist is then developed. This means the exposed wafer is brought into contact with a developing solution. For positive resist, the exposed areas are dissolved in the developer and for negative resist, the unexposed areas are dissolved leaving the SiO_2 surface uncovered in these areas. Sixth, after a hard bake, an etching process is used to remove the SiO_2 layer at selected regions where the resist has been removed. Two basic types of etching are chemical etching and plasma etching. Seventh, after stripping the resist, a hole or passageway is etched in the silicon wafer itself at the location where the SiO_2 has been removed. This can be done using a chemical etch consisting of a mixture of nitric acid and hydrofluoric acid.[55] It is important to note that holes can be various shapes and sizes. Depending on the orientation of the crystal planes in the silicon, holes with $53.4°$ wall angles are possible as well as holes with vertical walls. And lastly, the individual chips are then cut from the circular silicon wafer. The square or rectangular chips can range from 5 to 15 mm on a side.[55] Also, it is possible to fuse two or more chips together after they have been individually processed.